Investigation of new particle formation at the summit of Mt. Tai, China

Ganglin Lv[1], Xiao Sui[1], Jianmin Chen[1,2*], Rohan Jayaratne[3], Abdelwahid Mellouki[1,4]

[1]School of Environmental Science and Engineering, Environment Research Institute, Shandong University, Jinan, Shandong 250100, China

[2]Shanghai Key Laboratory of Atmospheric Particle Pollution and Prevention (LAP3), Institute of Atmospheric Sciences, Fudan University, Shanghai 200433, China

[3]International Laboratory for Air Quality and Health, Science and Engineering Faculty, Queensland University of Technology, GPO Box 2434, Brisbane QLD 4001, Australia

[4]Institut de Combustion, Aérothermique, Réactivité et Environnement, CNRS, 45071 Orléans cedex 02, France

Correspondence to: Jianmin Chen (jmchen@fudan.edu.cn); Tel.: +86 53188363711; fax: +86 531 88361990

Abstract. To date few comprehensive field observations of new particle formation (NPF) have been carried out at mountain-top sites in China. In this study, simultaneous measurements of particle size distribution, trace gases, meteorological parameters, mass concentration and chemical composition of $PM_{2.5}$ were performed at the summit of Mt. Tai (1534 m ASL) from 25 July to 24 August 2014 (Phase I), 21 September to 9 December 2014 (Phase II), and 16 June to 7 August 2015 (Phase III), to investigate characteristics and favorable conditions of NPF in a relatively clean mountain-top environment. The NPF events were identified based on particle size distribution measured by the neutral cluster and air ion spectrometer (NAIS), and 66 such events were observed during a period of 164 days — corresponding to an occurrence frequency of 40%. The formation rates of 3 nm particles (J_3) and growth rates (GR) were in the ranges of 0.82-25.04 cm^{-3} s^{-1} and 0.58-7.76 nm h^{-1}, respectively. On average, the condensation sink (CS), O_3 concentration, air temperature and relative humidity were lower, whereas the SO_2 concentration was higher on NPF days than that on non-NPF days. The CS on Mt. Tai was in a low level and lower CS was critical for NPF. NPF events were common when wind came from east-southeast and west-southwest, which was probably associated with relatively lower CS in the east-southeast and higher SO_2 concentration in the west-southwest. O_3 was not a governing factor for NPF in this study, and high level of NO_x concentration might be responsible for the decreased O_3 concentration on NPF days. Three categories of backward trajectories were classified, among which the continental air mass was the majority. The continental air mass passing through more polluted areas (denoted as Type I) was in favor of NPF because of enhanced SO_2 concentration and potential ammonia with it. An in-depth analysis of SO_2 indicated that sulfuric acid was a dominant precursor on Mt. Tai, meanwhile biogenic organics released from ambient forests in warm seasons and anthropogenic VOCs emitted from domestic heating in cold seasons also promoted NPF.

Keywords. New particle formation; Mountain observation; Favorable conditions; Precursor species

1 Introduction

Atmospheric aerosols play a critical role in affecting global radiation forcing and climate (Kazil et al., 2010), directly through scattering and absorption of solar radiation, and indirectly by modifying cloud properties and lifetimes as the potential cloud condensation nuclei (CCN) (Kuang et al., 2010). Aerosol particles are also involved in several atmospheric chemistry processes such as enhancing haze and decreasing visibility, which are associated with air quality (Guo et al., 2014). In addition, aerosol particles can harm human health by inhalation (Han, 2012;Butt et al., 2016). Previous studies have shown that the nucleation of atmospheric gas-phase precursors and subsequent growth to larger particles, widely known as new particle formation (NPF), is the largest source of atmospheric aerosol particles (Zhang et al., 2012). Field observations have exhibited that NPF typically increase the particle number concentration by a factor of two to ten (Gong et al., 2010). Modeling studies also revealed that NPF accounted for 5-50% of CCN in the lower boundary layer (Spracklen et al., 2008). An in-depth study of the process of NPF and its effects contribute significantly to the pollution controls of atmospheric aerosols in China.

With development of instruments that measure particle size distribution, NPF events have been widely observed all over the world in recent decades. These observation sites include northern-most sub-arctic, remote boreal forests, industrialized agricultural regions, high-iodine coastal environments, and polluted urban areas (Dal Maso et al., 2002). The frequency of NPF events varies significantly between different locations. For example, Hallar et al. (2011) reported that NPF events in urban areas in Pittsburgh, USA occurred on about 35-50% during the observation period, whereas the corresponding values at the remote background sites in Finland and Sweden were just 2-27%. Manninen et al. (2010) found that the frequency of NPF events ranged from 21% to 57% at twelve field sites around Europe, and the number of observed NPF days was closely related to the regional atmospheric conditions. In addition, the frequency of NPF events in a location is not constant. Wu et al. (2007) showed that NPF events occurred on 50%, 20%, 35%, and 45% of days in spring, summer, autumn and winter in Beijing.

In the past decade, many studies on NPF have been carried out in China. NPF events were firstly reported in China in 2004 by Wehner et al. (2004) who used a Twin Differential Mobility Particle Sizer (TDMPS). Soon after, Liu et al. (2008) observed NPF at a rural/coastal site in XinKen (Guangdong Province). In 2005, Gao et al. (2009) investigated the occurrence of NPF in a suburban environment in the Yangtze River delta using a Wide-range Particle Spectrometer (WPS). Thereafter, several observations related to NPF have been widely reported in urban, suburban and rural environments around China (An et al., 2015;Wang et al., 2011;Peng et al., 2014). At the remote high elevation sites, NPF might reveal some specific characteristics. Lots of mountain studies of NPF ranged around world so far, such as Mount Norikura in Japan, Jungfraujoch (3580 m asl) in Switzerland, Mt. Werner in America, and Himalayas in Nepal (Hallar et al., 2011;Chiharu et al., 2008;Weingartner et al., 1999;Venzac et al., 2008). At present, there have not many such observations on mountain-top sites

in China. Until 2008, Zhang et al. (2016) firstly conducted an observation of NPF on Mt. Huang, China (1840 m ASL) with WPS instrument. However, these recent mountain-top studies in China were subjected to great constraint in measurement methods. In this study, neutral cluster and air ion spectrometer (NAIS) was used, which could detect particle size distribution down than 3 nm. The NAIS greatly avoided the misleading interference of primary emission, and it exerted more actual particle formation sizes (Jayaratne et al., 2017).

Particle formation and growth rates vary with field environments. A review carried out by Kulmala et al. (2004) found that the typical formation rate was in the range of 0.01-10 cm^{-3} s^{-1}. In urban areas it may be about 100 cm^{-3} s^{-1}, while in coastal zones it can be as high as 10^4-10^5 cm^{-3} s^{-1}. Typical growth rate of newly formed particles ranges from 1 to 20 nm h^{-1}, and at some coastal areas it is as high as 200 nm h^{-1}.

Chemical mechanisms and precursor species related to NPF still remain uncertain, particularly under highly complicated atmospheric environments in China. Previous studies have shown that sulfuric acid, ammonia, organics, and iodide species in the atmosphere were involved in the nucleation process under specific environments. Gaseous sulfuric acid is commonly the critical candidate participating in binary, ternary and ion induced nucleation (Boy et al., 2005;Wang et al., 2011;Zhang, 2010;Saunders et al., 2010;Allan et al., 2015). It has also been shown that nucleation rate is a function of sulfuric acid concentration with a power dependency exponent, and its exponent varies significantly between different nucleation theories (Kulmala et al., 2006;Wang et al., 2011). However, presence of single sulfuric acid is always not enough to explain NPF in the atmosphere. Earlier studies indicated that ammonia and organics could enhance nucleation by stabilizing sulfuric acid-water clusters, and organics might exert more effectively at low concentration (Li et al., 2017). In Zhang et al. (2004) and Zhang (2010), they showed that sulfuric acid and organic acid could form a stable organic acid-sulfuric acid complex which could efficiently reduce the nucleation barrier.

Besides precursors, NPF in the atmosphere reveals the sensitivity of other factors, such as pre-existing particles, meteorological conditions, and air mass transport. Pre-existing particles contribute to a major sink for newly formed particles, and the large particle surface areas even probably act as governing factor of NPF, such as research of Cai et al. (2017) in Beijing. Comprehensive investigations of these factors on NPF in China have mainly been conducted in urban, suburban, and rural environments. Since mechanisms of NPF under the heavily polluted conditions is significantly different from that under relatively clean conditions (Kulmala et al., 2016;Hu et al., 2016;Wang et al., 2013), the comprehensive investigation of NPF on relatively clean mountain-top site of Mt. Tai is of great important.

In this paper, we present the results of intensive field observations at the summit of Mt. Tai (1534 m ASL), which is a relatively clean mountain-top environment. This study was based on simultaneous measurements of particle size distribution, meteorological parameters, gaseous species, mass concentration and chemical composition of $PM_{2.5}$ during three campaigns (25 July to 24 August 2014, Phase I; 21 September to 9 December 2014, Phase II; 16 June to 7 August 2015, Phase III). The general characteristics of NPF events, such as their start times, formation and growth rates were discussed based on a more

reliable nanometer instrument of NAIS that can detect particles down to actual formation sizes. We explored the favorable conditions for NPF by analyzing factors, such as condensation sinks (CS) and sources, meteorological conditions, and long-range air mass transport on NPF-days and non-NPF days. Besides, potential precursor species were also investigated in this study.

2 Methods

2.1 Site description

The observations were conducted at the summit of Mt. Tai (36.25 °N, 117.1 °E, 1534 m ASL), located nearly the centre of Shandong Province, eastern China. Mt. Tai is one of the highest mountains near the East China Sea on the transport path of the Asian continental outflow (Li et al., 2011), adjacent to the Bohai Sea (B-S) and Yellow Sea (Y-S). The field site is just at the summit of Mt. Tai, and its surroundings are dominated by dense vegetation in summer and autumn with few anthropogenic primary emission nearby. The nearest mid-size city, Tai'an with a population of 670,000, is located approximately 15 km away to the south and southeast. The city of Ji'nan (population: 2,800,000), capital of Shandong Province, is 60 km to the north. During daytime, the summit of Mt. Tai reaches close to the top of the planetary boundary layer (PBL), and the observation site is representative of the region (Zhang et al., 2014;Sun et al., 2016). All the instruments were installed inside a large trailer home, sampling through short inlet tubes outside the container at a height of about 3 m above the ground level.

2.2 Measurement techniques

Two types of particle size distribution instruments, namely neutral cluster and air ion spectrometer (NAIS) and wide-range particle spectrometer (WPS), two gas monitors (SO_2 and O_3), an instrument for mass concentration of $PM_{2.5}$ and a monitor for chemical composition in $PM_{2.5}$ were used in this study. In addition, meteorological parameters including air temperature (T), relative humidity (RH), wind speed (WS), wind direction (WD) and visibility were also recorded in real time.

The NAIS is a multichannel nanometer aerosol instrument which can measure the size distribution of aerosol particles and ions (charged particles and cluster ions) of both polarities simultaneously. The aerosol particle distribution of NAIS is in the size range of 2─40 nm, and the ion distribution is in the electric mobility range of 0.0013-3.2 $cm^2\ V^{-1}\ s^{-1}$ (equivalent to particle Millikan diameters of 0.8-40 nm). The instrument consists of two multichannel electrical mobility analyzer columns, one for each polarity. The aerosols are classified according to electrical mobility and measured with an array of twenty-one electrometers per column. The total time of each measurement cycle was set at 5 min, comprising of sampling intervals as follows: particles 120 s, ions 120 s and offset 60 s. Analysis of characteristics of NPF in the study was mainly based on the data measured by NAIS.

The WPS is a high-resolution aerosol spectrometer which combines a differential mobility analyzer (DMA), a

condensation particle counter (CPC) and a laser light scattering (LPS). The diameter range of WPS was from 10 to 10,000 nm, and 48 channels were used in the DMA and 24 channels were used for the LPS. The scan time for the entire size range was set to 5 min.

The concentration of SO_2 in the atmosphere was measured with a pulsed ultraviolet fluorescence analyzer (Model 43C, Thermo Electron Corporation-TEC), and O_3 was measured with an ultraviolet photometric analyzer (Model 49C, TEC). Mass concentration of $PM_{2.5}$ was detected by a monitor utilizing a combination of beta attenuation and light scattering technology (Model 5030 SHARP Monitor, Thermo Fisher Scientific), and chemical composition of $PM_{2.5}$ was measured by a Monitor for Aerosols and Gases (MARGA, ADI20801, Applikon-ECN, Netherlands). Meteorological data were obtained in real time with an automatic meteorological station (MILOS520, Vaisala, Finland).

2.3 Data analysis

2.3.1 Formation rate, growth rate and condensation sink

In this study, particles in the size range of 3-20 nm was regarded as nucleation particles, and the formation rate of nucleation mode particles, $J_{3\text{-}20}$, can be expressed (Dal Maso et al., 2005) as:

$$J_{3\text{-}20} = \frac{dN_{3\text{-}20}}{dt} + F_{\text{CoagS}} + F_{\text{growth}} \quad (1)$$

where $dN_{3\text{-}20}/dt$ is the net rate of increased nucleation mode particles, F_{CoagS} is the coagulation loss and F_{growth} is the loss of particles growing out of size range. In our observation, the F_{growth} term could be neglected because particles growing beyond 20 nm before formation ended was relatively rare. In addition, the formation rate of 3 nm particles, J_3, was also calculated from the NAIS data (Sihto et al., 2006;Kulmala et al., 2012) by using equation (2):

$$J_3 = \frac{dN_{3\text{-}6}}{dt} + \text{CoagS}_{Dp=4\text{ nm}} \cdot N_{3\text{-}6} + \frac{1}{3\text{ nm}}\text{GR}_{3\text{-}6} \cdot N_{3\text{-}6} \quad (2)$$

where $\text{CoagS}_{DP=4\text{ nm}}$ represents the coagulation sink of 4 nm particles, an approximation for the interval of 3-6 nm particles. $\text{GR}_{3\text{-}6}$ and $N_{3\text{-}6}$ denote the particle growth rate and particle number concentration between 3 and 6 nm, respectively.

The particle growth rate, GR, was determined by the maximum concentration method (Kulmala et al., 2012):

$$\text{GR} = \frac{\Delta D_{\text{m}}}{\Delta t} = \frac{D_{\text{m2}} - D_{\text{m1}}}{t_2 - t_1} \quad (3)$$

where D_{m1} and D_{m2} are the geometric median diameters of representative particles at the start time t_1 and the end time t_2, respectively.

Condensation sink, CS, determines the rate of molecules condensing on the pre-existing aerosols, and it is given by equation (4) (Dal Maso et al., 2005;Kulmala et al., 2001):

$$\text{CS} = 2\pi D \sum_i \beta_{Mi}\, Dp_i\, N_i \quad (4)$$

where D is the diffusion coefficient for sulfuric acid, and β_{M} is the size-dependent transitional correction factor.

2.3.2 Sulfuric acid proxy

Direct measurement of gas-phase sulfuric acid concentration was not available in this study. Instead, the predictive proxy for sulfuric acid ($[H_2SO_4]$) could be roughly estimated based on the solar radiation (SR), SO_2 concentration, CS and RH (Mikkonen et al., 2011):

$$[H_2SO_4] = 8.21 \cdot 10^{-3} \cdot k \cdot SR \cdot [SO_2]^{0.62} \cdot (CS \cdot RH)^{-0.13} \quad (5)$$

Here k is a temperature-dependent reaction rate constant, and the solar radiation is estimated from Hybrid Single Particle Lagrangian Integrated Trajectory (HYSPLIT) Model developed by the Air Resources Laboratory of U.S. National Oceanic and Atmospheric Administration (NOAA). The absolute values of sulfuric acid concentration contain some error with the real concentrations because of great uncertainty of solar radiation from HYSPLIT, but its diurnal variation pattern is acceptable.

3 Results and discussion

3.1 Classification and characteristics of NPF events

Basically, an NPF event could be defined as a distinct burst of new nucleation mode particles and subsequent growth of particles to larger size over a period of time (Dal Maso et al., 2005;Hallar et al., 2011;Wang et al., 2014a;Xiao et al., 2015). For the Mt. Tai observations in this study, neutral particles generally accounted for more than 95% of the total particles during NPF events, so the distribution of neutral particles would be emphatically discussed in this paper.

The data presented in this study covered three campaigns from 25 July to 24 August 2014 (Phase I), 21 September to 9 December 2014 (Phase II), and 16 June to 7 August 2015 (Phase III) at the summit of Mt. Tai. Observations over the 164 days showed that NPF events occurred on 66 days, corresponding to an occurrence frequency of 40%. NPF events were frequently observed throughout the measurement campaigns, with a highest occurrence frequency of 56% during the Phase II. In contrast, the average frequency was only 21% during the other two Phases. The difference was mainly attributed to the rainy/foggy conditions of Phases I and III, which played the predominating role of hindering NPF.

In Fig. 1a, one month's set of continuous data from 10 November to 9 December 2014 for intensive NPF events were picked to take a closer look at NAIS spectrogram, and the shaded areas represented NPF days. The spectrogram showed clear banana profiles on NPF days, and most events leveled off at about 30 nm. These NPF events usually lasted hours, implying that NPF events mainly occurred on the regional scale.

In this study, we defined the observed start times of NPF events based on the significant enhancement of particle number concentration between 3 nm and 6 nm, $N_{3\text{-}6}$. Results showed that approximately 95% of NPF events initiated at 8:00-11:00 LT (local time) at the summit of Mt. Tai, which is in good agreement with many previous reports in China (Guo et al., 2012;An et al., 2015;Kulmala et al., 2016;Hao et al., 2015). The start times of NPF events at the summit of Mt. Tai were

mainly associated with the enhanced photochemical products in the early morning, generally corresponding to the sunrise. Since newly formed particles (about 1.4 nm) need some time to grow to the measurable diameter, the real start times of NPF events would be earlier than above observed times.

Table 1 lists the calculated parameters of all the NPF events observed at the summit of Mt. Tai, such as formation rate of nucleation mode particles, formation rate of 3 nm particles, growth rate, condensation sink, average sulfuric acid proxy concentration in the early morning (generally corresponding to the time period of 6:00-9:00 LT on Mt. Tai), SO_2 concentration (6:00-13:00 LT), and O_3 concentration (6:00-13:00 LT). Table 2 summarizes the averages, medians, 25th percentiles, 75th percentiles, minima and maxima of these parameters on the basis of Table 1. Table 3 compares the characteristics of NPF on Mt. Tai in the study with some other researches in China.

The net increase rates and formation rates of nucleation mode particles on Mt. Tai were in the range of 0.96-48.52 cm^{-3} s^{-1} and 1.10-57.43 cm^{-3} s^{-1}, respectively. On average, the coagulation loss accounted for 24.6% of nucleation mode particle formation, which was significantly smaller than the result in Beijing in Yue et al. (2010). Coagulation could decrease the number concentration of newly formed particles, and lower value of coagulation loss implied that NPF on Mt. Tai would contribute to higher CCN concentration. The maximum values of net increase rate, formation rate and SO_2 concentration all occurred on the same day—3 December 2014, and SO_2 concentration on this day was as high as 12.9±9.6 ppb. The formation rates J_3 varied from 0.82 to 25.04 cm^{-3} s^{-1}, and their median, 25th percentile, and 75th percentile were 6.15, 3.31, and 9.41 cm^{-3} s^{-1}, respectively. On 3 December 2014, J_3 also peaked, suggesting that sulfuric acid was the governing precursor for the NPF event on this day. As shown in Table 3, the particle formation rate at the summit of Mt. Tai was significantly higher than that on the hillside of Mt. Tai Mo Shan (0.97-10.2 cm^{-3} s^{-1}) and on the top of Mt. Huang (0.09-0.30 cm^{-3} s^{-1}) (Guo et al., 2012;Zhang et al., 2016), but lower than the results in Beijing and Shanghai (Xiao et al., 2015;Wang et al., 2015). Besides, the observed formation rate on Mt. Tai was slightly higher than the rural and suburban sites in Table 3 (Liu et al., 2008;Yue et al., 2013;Qi et al., 2015). Precursor concentrations on Mt. Tai should not be abundant compared with megacities such as Beijing, but the lower level of CS (detailed discussion in Sect. 3.2) on Mt. Tai could be partially responsible for the relatively high formation rate in this study.

Growth rates $GR_{3\text{-}20}$ at the summit of Mt. Tai ranged from 0.58 to 7.76 nm h^{-1}, and the median, 25th percentile and 75th percentile were 1.55, 1.15 and 2.51 nm h^{-1}, respectively. Growth rate on Mt. Tai was comparable with some other mountain observations such as 1.5-8.4 nm h^{-1} at Mt. Tai Mo Shan, 1.42-4.53 nm h^{-1} on Mt. Huang, and 0.8-3.2 nm h^{-1} on Mt. Daban (Du et al., 2015;Guo et al., 2012;Hao et al., 2015;Zhang et al., 2016). Growth rates observed at the rural, suburban and urban sites were higher than these mountain observations shown in Table 3 (Yue et al., 2013;Liu et al., 2008;Gao et al., 2011;Qi et al., 2015;Xiao et al., 2015), suggesting that relatively clean mountain environments in this study contained insufficient vapors for subsequent particle growth.

3.2 Condensation sinks and sources of NPF

Classification of NPF events is associated with the persistent high concentration of nucleation mode particles, and occurrence of an NPF event is dependent on the competition between relevant sinks and sources. Newly formed particles are easily scavenged by larger pre-existing particles in the atmosphere, leading to their continual reduction in particle number concentration. On the other hand, sufficiently high concentration of low volatility vapors (precursors) contribute to persistent nucleation, generating new atmospheric particles. Therefore, the CS and precursors are the key factors for NPF. As reported by Wang et al. (2011) and Guo et al. (2012), the lower CS and higher precursor concentrations are favorable to NPF. It is difficult to quantify the balance between the CS and precursors, and NPF events could be observed in many kinds of environments. For example, Kulmala et al. (2016) reported that NPF could occur in some highly polluted Chinese megacities with high aerosol loadings. Zhu et al. (2014) showed that NPF events were observed in Qingdao City, where the high concentration of gaseous pollutants might offset the effect of large CS. In a semi-rural location in India, Kanawade et al. (2014) also demonstrated that NPF events were not limited by low value of CS alone. Therefore, the detailed analysis of sinks and sources in a specific site is of great importance for NPF.

In this study, CS on NPF days varied from 0.1×10^{-2}-28.4×10^{-2} s^{-1}, corresponding to the median, 25th percentile, and 75th percentile of 0.9×10^{-2} s^{-1}, 0.5×10^{-2} s^{-1} and 1.7×10^{-2} s^{-1}, respectively. The CS was much greater than 0.5×10^{-3}-3.5×10^{-3} s^{-1} in Hyytiälä, Finland (Dal Maso et al., 2005), but significantly lower than that at many locations in China, such as 0.6×10^{-2}-8.4×10^{-2} s^{-1} in Beijing, 0.9×10^{-2}-3.9×10^{-2} s^{-1} in Nanjing, 0.9×10^{-2}-5.3×10^{-2} in Qingdao, and 1.0×10^{-2}-6.2×10^{-2} s^{-1} in Hong Kong (Zhang et al., 2011;Gao et al., 2012;Guo et al., 2012;An et al., 2015;Herrmann et al., 2014;Zhu et al., 2014). Overall, the general atmospheric environment at the summit of Mt. Tai is relatively clean in China with low particle loadings. The hourly average CS on non-NPF days was always higher than that on NPF days, being $(2.0\pm0.5)\times10^{-2}$ s^{-1} and $(1.4\pm0.5)\times10^{-2}$ s^{-1}, respectively. The result indicated that occurrence of NPF at the summit of Mt. Tai was significantly influenced by lower CS.

Gas-phase sulfuric acid has been identified as the most important precursor for nucleation. Because direct emission of sulfuric acid is negligible at the summit of Mt. Tai, photochemical reactions of SO_2 would be the significant source for sulfuric acid in the atmosphere. As shown in Fig. 2a, SO_2 concentration showed sharp increase at sunrise, and almost all the hourly average SO_2 concentrations on NPF days were higher than the corresponding values on non-NPF days (except for the slightly lower values at 1:00 LT and 3:00 LT). It indicated that sulfuric acid participated in NPF and played an important role for the initiation of NPF events.

Figure 1 also showed visual correlations between particle number size distribution, gas species, meteorological parameters, and $PM_{2.5}$ concentration. As discussed above, higher SO_2 concentration can increase the occurrence possibility of NPF events. The frequent NPF events in the early December, for instance, could be attributed to enhanced SO_2 concentration. In

Fig. 1c, it was noteworthy that temperature suddenly dropped from 1.3 ℃ to -9.4 ℃ on 30 November 2014. After several days, an exceptionally high SO_2 concentration was observed (7.1 ±7.2 ppb) at the summit of Mt. Tai (marked in violet block in Fig. 1), and frequent NPF events occurred during this period. A possible reason for this observation might be the entrainment of SO_2 from coal or petroleum combustion in the upwind region when temperature abruptly changed (Li et al., 2015a;Li et al., 2015b).

In this study, a proxy based on SR, SO_2 concentration, CS and RH was used to roughly estimate the magnitude of sulfuric acid concentration in the atmosphere. In the calculations, the average sulfuric acid proxy concentration of all NPF days was 5.23×10^6 cm^{-3} during 6:00-9:00 LT, which could be comparable with 4.1×10^6 cm^{-3} in Beijing but much lower than 2.3×10^7-6.4×10^7 cm^{-3} in Shanghai and 6.6×10^7-7.8×10^7 cm^{-3} in Nanjing (Wang et al., 2014b;Wang et al., 2015;Xiao et al., 2015). Severely polluted sites generally correspond to elevated CS, and thus will require a higher concentration of precursors to initiate nucleation to a certain. The fact could be indirectly reflected through many oversea studies in which NPF events were observed at clean or moderately-polluted sites in the presence of lower sulfuric acid concentration (Dal Maso et al., 2005;Boy et al., 2005). The lower initial sulfuric acid proxy concentration in this study could be partly explained by relatively lower CS on Mt. Tai.

As the most critical nucleation precursor, sulfuric acid is associated with freshly nucleated particles. Further investigation in this study found that sulfuric acid proxy concentration showed the clear positive correlation with $N_{3\text{-}6}$ on many NPF days, consistent with earlier reports (Kulmala et al., 2006;Wang et al., 2011;Guo et al., 2012). The positive correlation was another evidence that sulfuric acid played the dominant role in NPF at the summit of Mt. Tai, as foregoing discussion. As an example, $N_{3\text{-}6}$ reflected a best relationship (R^2 =0.975) with sulfuric acid proxy concentration between 6:00 and 14:00 LT on the NPF day of 14 October 2014 (Fig. 3). After 14:00 LT, SO_2 concentration increased sharply (a change from 2.6 ppb at 14:00 LT to 19.1 ppb at 15:00), resulting in a lack of correlation between SO_2 concentration and $N_{3\text{-}6}$ in the afternoon. In principle, the increase of sulfuric acid concentration should take place earlier than the increase of $N_{3\text{-}6}$. However, there were some NPF days with zero or negative time delay in this study, such as on 14 October 2014 in Fig. 3. Wang et al. (2011) indicated that the pre-formed nucleation mode particles and rapid particle growth might account for such zero or negative time delay.

Wind direction reflected the local situation for air mass, which could indirectly verify the competition between sinks and sources when NPF events occurred. Throughout the three campaigns, the dominant wind directions were easterly and westerly, being the main directions of 40 º-110 ºand 220 º-300 º(Fig. 4). Compared with non-NPF days, the wind direction on NPF days had narrower ranges in the east-southeasterly (85 º-110 º) and west-southwesterly directions (250 º-300 º), as shown in Fig. 4. The CS on Mt. Tai changed with wind direction, and the average CS in the wind directions between 40 ºand 110 º (2.0×10^{-2} s^{-1}) were almost twice as high as that in the wind directions between 220 ºand 300 º(1.1×10^{-2} s^{-1}). It indicated that air mass from the west of Mt. Tai was usually cleaner than that from the east. For the easterly wind, it was noted that the CS

was a relatively small value when the wind came from the east-southeast direction, partly explaining the frequent occurrence of NPF events in this particular direction. SO_2 concentrations were almost evenly distributed with wind direction in this study, except for the west-southwest direction which corresponded to an elevated SO_2 concentration of 4.3 ppb on average. In contrast, the average SO_2 concentration were only 2.0 ppb for the adjacent wind directions between 220 ° and 350 °. This suggested that the potential sources in the west-southwest direction contributed to a greater likelihood of NPF events.

O_3 can directly react with VOCs or indirectly affect sulfuric acid formation via hydroxyl and hydroperoxy radicals (Berndt et al., 2010;Gómez Martín et al., 2013;Sorribas et al., 2015;Guo et al., 2012), and thus O_3 in the atmosphere may play a role in NPF theoretically. Previous researches showed that the elevated O_3 concentration was beneficial to the occurrence of NPF events (An et al., 2015;Guo et al., 2012;Zhang et al., 2016;Huang et al., 2016), and our results did not directly show similar phenomenon. The average O_3 concentrations on NPF days and non-NPF days were 40 ppb and 47 ppb, respectively, and the hourly average O_3 concentrations on NPF days were always lower than those on non-NPF days in Fig. 2b. The increasing rate of O_3 concentration on NPF days was significantly faster than that on non-NPF days after sunrise, implying that NPF did prefer the condition with abundant O_3. On the other hand, the lower O_3 concentration on NPF days also indicated that O_3 was not a key factor for NPF on Mt. Tai. Previous studies reported that there was an NO_x turnaround value of 10-15 ppb for the formation of O_3, and O_3 production appeared to decrease as NO_x when NO_x concentration exceeded the turnaround value (Lei, 2004). The average concentration of $NO+NO_2$ on NPF days and non-NPF days were 21 ppb and 20 ppb on Mt. Tai. The high level of NO_x concentration inversely contributed to O_3 formation to some extent, which was partially responsible for the decreased O_3 concentration on NPF days in Fig. 2b.

In Fig. 2b, the diurnal variations of O_3 concentration at the summit of Mt. Tai had two prominent features - a small trough in the early morning resulting from dry deposition and a broad peak in the afternoon due to formation by solar radiation. As Sun et al. (2016) reported, O_3 concentration between 02:00–05:00 LT reflected the regional baseline O_3. In this study, the average regional baseline O_3 was 42 ppb, being a relatively high level. The result should be related to the residual O_3 produced in the preceding afternoon in the boundary layer.

3.3 Meteorological conditions

Favorable meteorological conditions can promote the occurrence of NPF, especially when the precursor concentrations are insufficient in the atmosphere (Song et al., 2010). In this study, approximately 90 % of the NPF events occurred during clear or partial cloudy daytime. As discussed earlier in Sect. 3.1, NPF events initiated at the corresponding time of solar radiation rapidly increasing, suggesting the association between solar radiation and NPF.

The air temperature of all NPF days varied from -11.8 ℃ to 22.1 ℃ in this study. The daily temperature profiles were characterized by the expected cosine form of curve, and daily temperature generally oscillated less than 10 ℃ within a day. Temperature at the summit of Mt. Tai exhibited a clear seasonal behavior. As observed in Fig. 2c, the hourly average

temperatures on non-NPF days (10.7±1.1 ℃) were always higher than that on NPF days (7.0±1.8 ℃), indicating that NPF events at the summit of Mt. Tai favored the relatively low air temperature. The result was in good agreement with many previous observations at Mt. Tai Mo Shan (Guo et al., 2012), Mt. Huang (Zhang et al., 2016), and PUY in France (Rose et al., 2015), which all reported the correlation between lower temperature and NPF events. In Guo et al. (2012), it explained that the favorable lower temperature could enhance bind between sulfuric acid and water molecules. Li et al. (2017) also indicated that the strength (r) of lactic acid increased with decreasing temperature based on the molecular-scale study of interaction between lactic acid and nucleation precursors. Besides, the enhancement of NPF events in lower temperature was partly attributed to atmospheric vertical convection and enhanced matter transport.

The RH on NPF days ranged from 22% to 95%, and diurnal variation of RH was inversely correlated with solar radiation. The hourly average RH on NPF days (63±5 %) was always much lower than the corresponding value on non-NPF days (88±2%), and the maximum difference between two curves in Fig. 2d was as high as 30% at noon. An anti-correlation between NPF and RH can be identified at the summit of Mt. Tai, which is in agreement with the results in Beijing, Nanjing, Hong Kong, and Mt. Huang (An et al., 2015;Wang et al., 2014a;Shen et al., 2016;Zhang et al., 2016;Guo et al., 2012). The actual role of RH on NPF is still controversial and has not been resolved currently. Hamed et al. (2011) indicated that RH affected the source of NPF via decreasing solar radiation under high RH conditions. In contrast, simultaneous increasing CS (sink) under high RH conditions was also suggested as an explanation for the negative effect of RH (Hamed et al., 2011;Guo et al., 2012). Li et al. (2017) reported that the strength (r) of lactic acid in NPF events revealed sensitive to RH and increased with the decreasing RH, which was possibly associated with the hydration ability of sulfuric acid-base clusters.

3.4 Long-range air mass transport

To characterize the influence of long-range air mass transport on NPF at the summit of Mt. Tai, air mass backward trajectories for 72 h at 6:00 LT at 1535 m ASL were simulated by using the HYSPLIT model developed by the National Oceanic and Atmospheric Administration (NOAA) Air Resources Laboratory. Figure 5a illustrates the air mass backward trajectories of all NPF days, and Fig. 5b shows for all non-NPF days.

Based on the transport range and distance, the air mass backward trajectories were classified into three categories in Fig. 5: continental air mass (red), local air mass (green) and maritime air mass (magenta). The majority of transport pathways on NPF days were continental air mass, which accounted for 80% of the total air masses. The continental air mass on NPF days mainly came from northwest of the observation site, and largely originated from Siberia passing over the long distance across Mongolia, Inner Mongolia, Shanxi Province, Hebei Province, and Beijing. The local and maritime backward trajectories on NPF days accounted for 8% and 12% of the total trajectories, respectively. The local air mass was mainly from surrounding cities such as Jinan, Nanjing, Zhengzhou with shorter routes, whereas the maritime air mass originated over the Bohai Sea (E-S), Yellow Sea (Y-S) and East China Sea (E-S).

The ratios of continental air mass, local air mass and maritime air mass on non-NPF days were 63%, 12% and 25%, respectively. Overall, the local air mass accounted for the minimum percentage on both NPF and non-NPF days. It was noted that there were significantly lower ratio of maritime air mass and shorter routes over ocean areas on NPF days in Fig. 5. The phenomena were in line with Peng et al. (2014) in which non-NPF events were observed when air mass came from the clean ocean side at three coastal sites. Reason for this result was probably that the maritime air mass could not provide enough precursors for NPF.

As mentioned above, the continental air mass dominated throughout the observations. According to its transport regions, more polluted continental air mass (Type I) and relatively cleaner continental air mass (Type II) were denoted in this study. Air mass of Type I passed though the heavily polluted areas of Beijing, Hebei Province, Shanxi Province, Henan Province, and Shaanxi Province before reaching the observation site, which probably carried a substantial fraction of extra matters. Air mass of Type II was either from south China or transported over the Bohai Sea (B-S) and Yellow Sea (Y-S), and thus it represented relatively cleaner air mass. In this study, four-fifths of continental air masses on NPF days were Type I, whereas Type I only accounted for two-fifths on non-NPF days. The significant difference implied that the Type I air mass passing through the heavily polluted areas might be in favor of NPF.

In order to further verify the speculation that the Type I air mass was favorable for NPF, Fig. 6 illustrates the average chemical composition of $PM_{2.5}$ and SO_2 concentration in Type I and Type II on NPF days. The average mass concentrations of $PM_{2.5}$ in Type I and Type II were 33 μg m^{-3} and 23 μg m^{-3}, and Type I air mass was obviously more polluted than Type II. It was noted that a prominent increase of SO_2 concentration was found in Type I, being average SO_2 concentration of 3.9 ppb and 1.2 ppb, respectively. Higher SO_2 concentration suggested that sulfuric acid participated in NPF and played an important role in it, which could also be reflected by the largest enhancement mixing ratio of sulfate in $PM_{2.5}$ in Type I. In addition, the significantly elevated mixing ratios of ammonium and nitrate were found in Type I, suggesting that these polluted areas might be N-rich and potential ammonia also promoted efficient NPF in Type I.

Long-range air mass transport reflects a regional picture before nucleation, so it is of great importance for NPF. An NPF event on 11 November 2014 was picked as a case study to further explore the influence of long-range air mass transport. The time series of particle size distribution, trace gases, chemical composition and mass concentration of $PM_{2.5}$ on this day are illustrated in Fig. 7.

In the early morning on 11 November 2014, the average concentrations of SO_2 and $PM_{2.5}$ were 1.7 ppb and 90 μg m^{-3}, respectively. Low level of SO_2 concentration and extremely high level of $PM_{2.5}$ concentration made atmospheric nucleation almost impossible. However, an NPF event was observed around noon, and the observed start time showed an obvious time delay compared with the general start time of 8:00-11:00 LT in Set. 3.1. In Fig. 7, it found the phenomena of clear increase in SO_2 concentration, decrease in $PM_{2.5}$ concentration and change in chemical composition of $PM_{2.5}$ simultaneously at about 10:00 LT. The observation site of Mt. Tai is located on the mountain top without any stationary source nearby, and this

abrupt changes may suggest that there was another air mass transported to the site, contributing to this unexpected NPF event. During 6:00-9:00 LT, the average mass concentrations of sulfate, ammonium, nitrate, OC and EC in $PM_{2.5}$ were 4.1, 4.6, 4.1, 7.6 and 0.7 μg m^{-3}, respectively. In contrast, their average concentrations shifted to 13.1, 11.2, 11.1, 10.0 and 0.2 μg m^{-3} during 11:00-18:00 LT. The mixing ratio of sulfate in $PM_{2.5}$ increased significantly before and after 10:00 LT, suggesting that the new transport air mass was sulfur-rich. Dual effects of elevated precursor (sulfuric acid) concentration and decreased pre-existing particle loadings were responsible for this NPF event.

In order to verify above speculation, air mass backward trajectories for 72 h at 1535 m ASL at 14:00, 12:00, 10:00, 8:00 and 6:00 LT on 11 November 2014 are shown in Fig. 8. It illustrates that the origin of transport air mass shifted from eastern China (Jiangsu and Anhui Provinces, lines A and B) to western China (lines C, D and E) at about 10:00 LT, which was in agreement with the earlier analysis in Fig. 7. The latter air mass backward trajectories (line C, D and E) passed through the heavily polluted areas, such as Shanxi and Shaanxi Provinces, before reaching the site of Mt. Tai. Those polluted areas were rich in SO_2, leading to the enhanced precursors for NPF.

3.5 Potential governing factors for NPF

NPF events at the summit of Mt. Tai revealed an obvious seasonal distribution. The occurrence frequency in summertime was strongly associated with atmospheric humidity, and the rainy/foggy conditions were a critical limiting factor for NPF in summertime. The nucleation mode particle concentrations were more fluctuant in summertime than other two seasons, which was possibly caused by heterogeneity of precursors. In autumntime and wintertime, the effect of meteorological conditions was not such overwhelming, and the precursor species and particle sinks played the key roles for NPF.

Earlier discussion of SO_2 in this study indicated that sulfuric acid played a dominant role in NPF at the summit of Mt. Tai. Highly large formation rate was observed in this study, but it could be explained by single sulfuric acid currently because of insufficient sulfuric acid concentration in the atmosphere. Zhang et al. (2004) showed that the organic acid-sulfuric acid system had a reduced nucleation barrier, and nucleation could be promoted several times in the presence of sub-ppb level of organics. Mt. Tai in this study has a high percentage of forest-covered lands, and thus abundant biogenic organics are theoretically released in warm seasons. Apart from sulfuric acid, biogenic organics most probably acted as the important precursors of NPF on Mt. Tai in warm seasons. In cold seasons, the release of biogenic organics might be reduced, but emissions of anthropogenic VOCs and SO_2 would be enhanced because of domestic heating in the region, contributing to the NPF in winter.

4. Conclusions

For the NPF issue, although a few observational results have been reported in China, to date very few researches conducted the comprehensive analysis of favorable conditions that gave rise to NPF events on mountain-top sites, not to mention

investigating characteristics of NPF based on the improved instruments. A comprehensive investigation of NPF was conducted at the summit of Mt. Tai (1534 m ASL), eastern China, from 25 July to 24 August 2014 (Phase I), 21 September to 9 December 2014 (Phase II) and 16 June to 7 August 2015 (Phase III), mainly using an NAIS instrument that could detect particles at smaller sizes.

During the 164 days, 66 NPF events were identified, giving an occurrence frequency of 40%. Approximately 95% of NPF events initiated at 8:00-11:00 LT, coincided with many previous reports in China. The J_3, $J_{3\text{-}20}$, and growth rates were in the range of 0.82-25.04 cm^{-3} s^{-1}, 1.10-57.43 cm^{-3} s^{-1}, and 0.58-7.76 nm h^{-1}, respectively. In comparison with other studies in China, the formation rate at the summit of Mt. Tai was subjected to the relatively high levels, which was partially attributable to the lower CS on Mt. Tai. In contrast, the lower growth rate suggested that precursors for particle growth were probably insufficient.

On average, the CS, O_3 concentration, T and RH were lower, whereas SO_2 concentration was higher on NPF days than that on non-NPF days. The CS on Mt. Tai was significantly lower compared with many other locations in China, and lower CS was one of critical factors for NPF. East-southeasterly (85 º-110 º) and west-southwesterly winds (250 º-300 º) dominated on NPF days, and relatively lower CS in the east-southeast and higher SO_2 concentration in the west-southwest were partially responsible for NPF. Elevated O_3 concentration was favorable for NPF, but O_3 was not a governing factor for NPF on Mt. Tai. The high level of NO_x concentration on Mt. Tai was adverse to O_3 formation, probably leading to the decreased O_3 concentration on NPF days. Lower T and lower RH were expectedly observed on NPF days in the study, which were in good agreement with previous results in other sites.

Three categories of backward air masses were classified on Mt. Tai, and they were continental air mass, local air mass and maritime air mass. The continental air mass was the majority on both NPF days and non-NPF days, and it was divided as Type I (more polluted continental air mass) and Type II (relatively cleaner continental air mass). An in-depth analysis showed that Type I air mass was in favor of NPF because the higher SO_2 concentration and potential ammonia were carried with it.

Sulfuric acid was identified as a dominant precursor of NPF at the summit of Mt. Tai, but its concentration was not sufficient to explain the highly large formation rate in this study. Abundant forest-covered Mt. Tai implied that considerable biogenic organics might be released in warm seasons and participated in NPF. In addition, increasing anthropogenic VOCs and SO_2 in the region could promote NPF in cold seasons. Further measurement of organics is still needed to explore what kind of organics participates in NPF.

Acknowledgements. This work was supported by National Natural Science Foundation of China (No. 41375126), Mount Tai Scholar Grand (ts20120552), Cyrus Tang Foundation (No.CTF-FD2014001), Ministry of Science and Technology of China (SQ2016ZY01002231, 2014BAC22B01), and Marie Skłodowska-Curie Actions (H2020-MSCA-RISE-2015-690958).

References

Allan, J. D., Williams, P. I., Najera, J., Whitehead, J. D., Flynn, M. J., Taylor, J. W., Liu, D., Darbyshire, E., Carpenter, L. J., Chance, R., Andrews, S. J., Hackenberg, S. C., and McFiggans, G.: Iodine observed in new particle formation events in the Arctic atmosphere during ACCACIA, Atmos. Chem. Phys., 15, 5599-5609, 10.5194/acp-15-5599-2015, 2015.

An, J., Wang, H., Shen, L., Zhu, B., Zou, J., Gao, J., and Kang, H.: Characteristics of new particle formation events in Nanjing, China: Effect of water-soluble ions, Atmos. Environ., 108, 32-40, 10.1016/j.atmosenv.2015.01.038, 2015.

Berndt, T., Stratmann, F., Sipilä, M., Vanhanen, J., Petäjä, T., Mikkilä, J., Grüner, A., Spindler, G., Lee Mauldin Iii, R., Curtius, J., Kulmala, M., and Heintzenberg, J.: Laboratory study on new particle formation from the reaction OH + SO_2 : influence of experimental conditions, H_2O vapour, NH_3 and the amine tert-butylamine on the overall process, Atmos. Chem. Phys., 10, 7101-7116, 10.5194/acp-10-7101-2010, 2010.

Boy, M., Kulmala, M., Ruuskanen, T. M., Pihlatie, M., Reissell, A., Aalto, P. P., Keronen, P., Dal Maso, M., Hellen, H., Hakola, H., Jansson, R., Hanke, M., and Arnold, F.: Sulphuric acid closure and contribution to nucleation mode particle growth, Atmos. Chem. Phys., 5, 863-878, 10.5194/acp-5-863-2005, 2005.

Butt, E. W., Rap, A., Schmidt, A., Scott, C. E., Pringle, K. J., Reddington, C. L., Richards, N. A. D., Woodhouse, M. T., Ramirez-Villegas, J., Yang, H., Vakkari, V., Stone, E. A., Rupakheti, M., S. Praveen, P., G. van Zyl, P., P. Beukes, J., Josipovic, M., Mitchell, E. J. S., Sallu, S. M., Forster, P. M., and Spracklen, D. V.: The impact of residential combustion emissions on atmospheric aerosol, human health, and climate, Atmos. Chem. Phys., 16, 873-905, 10.5194/acp-16-873-2016, 2016.

Cai, R., Yang, D., Fu, Y., Wang, X., Li, X., Ma, Y., Hao, J., Zheng, J., and Jiang, J.: Aerosol surface area concentration: a governing factor in new particle formation in Beijing, Atmos. Chem. Phys., 17, 12327-12340, 10.5194/acp-17-12327-2017, 2017.

Chiharu, N., Kazuo, O., Mizuka, K., Katsuji, M., and Yasunobu, I.: Nucleation mode particles in upslope valley winds at Mount Norikura, Japan: Implications for the vertical extent of new particle formation events in the lower troposphere, J. Geophys. Res., 113, 10.1029/2007jd009302, 2008.

Dal Maso, M., Kulmala, M., Lehtinen, K. E. J., Mäkelä, J. M., Aalto, P., and O'Dowd, D.: Condensation and coagulation sinks and formation of nucleation mode particles in coastal and boreal forest boundary layers, J. Geophys. Res., 107, 8097, 10.1029/2001JD001053, 2002.

Dal Maso, M., Kulmala, M., Riipinen, I., Wagner, R., Hussein, T., Aalto, P. P., and Lehtinen, K. E. J.: Formation and growth of fresh atmospheric aerosols : Eight Years of Aerosol Size Distribution Data from SMEAR II, Hyytiälä, Finland, Boreal Environ. Res., 10, 323-336, 2005.

Du, W., Sun, Y. L., Xu, Y. S., Jiang, Q., Wang, Q. Q., Yang, W., Wang, F., Bai, Z. P., Zhao, X. D., and Yang, Y. C.: Chemical

characterization of submicron aerosol and particle growth events at a national background site (3295 m a.s.l.) in the Tibetan Plateau, Atmos. Chem. Phys., 15, 10811-10824, 10.5194/acp-15-10811-2015, 2015.

Gómez Martín, J. C., Gálvez, O., Baeza-Romero, M. T., Ingham, T., Plane, J. M., and Blitz, M. A.: On the mechanism of iodine oxide particle formation, Phys. Chem. Chem. Phys., 15, 15612-15622, 10.1039/c3cp51217g, 2013.

Gao, J., Wang, T., Zhou, X., Wu, W., and Wang, W.: Measurement of aerosol number size distributions in the Yangtze River delta in China: Formation and growth of particles under polluted conditions, Atmos. Environ., 43, 829-836, 10.1016/j.atmosenv.2008.10.046, 2009.

Gao, J., Chai, F., Wang, T., and Wang, W.: Particle number size distribution and new particle formation (NPF) in Lanzhou, Western China, Particuology, 9, 611-618, 10.1016/j.partic.2011.06.008, 2011.

Gao, J., Chai, F., Wang, T., Wang, S., and Wang, W.: Particle number size distribution and new particle formation: New characteristics during the special pollution control period in Beijing, J. Environ. Sci., 24, 14-21, 10.1016/s1001-0742(11)60725-0, 2012.

Gong, Y., Hu, M., Cheng, Y., Su, H., Yue, D., Liu, F., Wiedensohler, A., Wang, Z., Kalesse, H., and Liu, S.: Competition of coagulation sink and source rate: New particle formation in the Pearl River Delta of China, Atmos. Environ., 44, 3278-3285, 10.1016/j.atmosenv.2010.05.049, 2010.

Guo, H., Wang, D. W., Cheung, K., Ling, Z. H., Chan, C. K., and Yao, X. H.: Observation of aerosol size distribution and new particle formation at a mountain site in subtropical Hong Kong, Atmos. Chem. Phys., 12, 9923-9939, 10.5194/acp-12-9923-2012, 2012.

Guo, S., Hu, M., Zamora, M. L., Peng, J., Shang, D., Zheng, J., Du, Z., Wu, Z., Shao, M., Zeng, L., Molina, M. J., and Zhang, R.: Elucidating severe urban haze formation in China, Proc. Natl. Acad. Sci. U S A, 111, 17373-17378, 10.1073/pnas.1419604111, 2014.

Hallar, A. G., Lowenthal, D. H., Chirokova, G., Borys, R. D., and Wiedinmyer, C.: Persistent daily new particle formation at a mountain-top location, Atmos. Environ., 45, 4111-4115, 10.1016/j.atmosenv.2011.04.044, 2011.

Hamed, A., Korhonen, H., Sihto, S.-L., Joutsensaari, J., Järvinen, H., Petäjä, T., Arnold, F., Nieminen, T., Kulmala, M., Smith, J. N., Lehtinen, K. E. J., and Laaksonen, A.: The role of relative humidity in continental new particle formation, J. Geophys. Res., 116, 909-926, 10.1029/2010jd014186, 2011.

Han, S.: Effect of Aerosols on Visibility and Radiation in Spring 2009 in Tianjin, China, Aerosol Air Qual. Res., 12, 211-217, 10.4209/aaqr.2011.05.0073, 2012.

Hao, J., Yin, Y., Li, X., Yuan, L., and Xiao, H.: Observations of Nucleation Mode Particles Formation and Growth on Mount Huang, China, Procedia Engineering, 102, 1167-1176, 10.1016/j.proeng.2015.01.242, 2015.

Herrmann, E., Ding, A. J., Kerminen, V. M., Petäjä, T., Yang, X. Q., Sun, J. N., Qi, X. M., Manninen, H., Hakala, J., Nieminen, T., Aalto, P. P., Kulmala, M., and Fu, C. B.: Aerosols and nucleation in eastern China: first insights from the new

SORPES-NJU station, Atmos. Chem. Phys., 14, 2169-2183, 10.5194/acp-14-2169-2014, 2014.

Hu, M., Shang, D., Guo, S., and Wu, Z.: Mechanism of New Particle Formation and Growth as well as Environmental Effects under Complex Air Pollution in China, Acta Chimica Sinica, 74, 385-391, 10.6023/a16020105, 2016.

Huang, X., Zhou, L., Ding, A., Qi, X., Nie, W., Wang, M., Chi, X., Petäjä, T., Kerminen, V.-M., Roldin, P., Rusanen, A., Kulmala, M., and Boy, M.: Comprehensive modelling study on observed new particle formation at the SORPES station in Nanjing, China, Atmos. Chem. Phys., 16, 2477-2492, 10.5194/acp-16-2477-2016, 2016.

Jayaratne, R., Pushpawela, B., He, C., Li, H., Gao, J., Chai, F., and Morawska, L.: Observations of particles at their formation sizes in Beijing, China, Atmos. Chem. Phys., 17, 8825-8835, 10.5194/acp-17-8825-2017, 2017.

Kanawade, V. P., Shika, S., Pöhlker, C., Rose, D., Suman, M. N. S., Gadhavi, H., Kumar, A., Nagendra, S. M. S., Ravikrishna, R., Yu, H., Sahu, L. K., Jayaraman, A., Andreae, M. O., Pöschl, U., and Gunthe, S. S.: Infrequent occurrence of new particle formation at a semi-rural location, Gadanki, in tropical Southern India, Atmos. Environ., 94, 264-273, 10.1016/j.atmosenv.2014.05.046, 2014.

Kazil, J., Stier, P., Zhang, K., Quaas, J., Kinne, S., O'Donnell, D., Rast, S., Esch, M., Ferrachat, S., Lohmann, U., and Feichter, J.: Aerosol nucleation and its role for clouds and Earth's radiative forcing in the aerosol-climate model ECHAM5-HAM, Atmos. Chem. Phys., 10, 10733-10752, 10.5194/acp-10-10733-2010, 2010.

Kuang, C., Riipinen, I., Sihto, S. L., Kulmala, M., McCormick, A. V., and McMurry, P. H.: An improved criterion for new particle formation in diverse atmospheric environments, Atmos. Chem. Phys., 10, 8469-8480, 10.5194/acp-10-8469-2010, 2010.

Kulmala, M., Dal Maso, M., Mäkelä, M., Pirjola, L., Väkevä, M., Aalto, P., Miikkulainen, P., and Hämeri, K.: On the formation, growth and composition of nucleation mode particles, Tellus B, 53, 479-490, 10.1034/j.1600-0889.2001.d01-33.x, 2001.

Kulmala, M., Vehkamäki, H., Petäjä, T., Dal Maso, M., Lauri, A., Kerminen, V. M., Birmili, W., and McMurry, P. H.: Formation and growth rates of ultrafine atmospheric particles: a review of observations, J. Aerosol Sci., 35, 143-176, 10.1016/j.jaerosci.2003.10.003, 2004.

Kulmala, M., Lehtinen, K. E. J., and Laaksonen, A.: Cluster activation theory as an explanation of the linear dependence between formation rate of 3 nm particles and sulphuric acid concentration, Atmos. Chem. Phys., 6, 787-793, 10.5194/acp-6-787-2006, 2006.

Kulmala, M., Petäjä, T., Nieminen, T., Sipila, M., Manninen, H. E., Lehtipalo, K., Dal Maso, M., Aalto, P. P., Junninen, H., Paasonen, P., Riipinen, I., Lehtinen, K. E., Laaksonen, A., and Kerminen, V. M.: Measurement of the nucleation of atmospheric aerosol particles, Nat. Protoc., 7, 1651-1667, 10.1038/nprot.2012.091, 2012.

Kulmala, M., Petäjä, T., Kerminen, V. M., Kujansuu, J., Ruuskanen, T., Ding, A. J., Nie, W., Hu, M., Wang, Z. B., Wu, Z. J., Wang, L., and Worsnop, D. R.: On secondary new particle formation in China, Front. Environ. Sci. Eng., 10, 08,

10.1007/s11783-016-0850-1, 2016.

Lei, W.: Chemical characterization of ozone formation in the Houston-Galveston area: A chemical transport model study, J. Geophys. Res., 109, 301, 10.1029/2003jd004219, 2004.

Li, H., Kupiainen-Määttä, O., Zhang, H., Zhang, X., and Ge, M.: A molecular-scale study on the role of lactic acid in new particle formation: Influence of relative humidity and temperature, Atmos. Environ., 166, 479-487, 10.1016/j.atmosenv.2017.07.039, 2017.

Li, T., Wang, Y., Li, W. J., Chen, J. M., Wang, T., and Wang, W. X.: Concentrations and solubility of trace elements in fine particles at a mountain site, southern China: regional sources and cloud processing, Atmos. Chem. Phys., 15, 8987-9002, 10.5194/acp-15-8987-2015, 2015a.

Li, W. J., Zhang, D. Z., Shao, L. Y., Zhou, S. Z., and Wang, W. X.: Individual particle analysis of aerosols collected under haze and non-haze conditions at a high-elevation mountain site in the North China plain, Atmos. Chem. Phys., 11, 11733-11744, 10.5194/acp-11-11733-2011, 2011.

Li, W. J., Chen, S. R., Xu, Y. S., Guo, X. C., Sun, Y. L., Yang, X. Y., Wang, Z. F., Zhao, X. D., Chen, J. M., and Wang, W. X.: Mixing state and sources of submicron regional background aerosols in the northern Qinghai–Tibet Plateau and the influence of biomass burning, Atmos. Chem. Phys., 15, 13365-13376, 10.5194/acp-15-13365-2015, 2015b.

Liu, S., Hu, M., Wu, Z., Wehner, B., Wiedensohler, A., and Cheng, Y.: Aerosol number size distribution and new particle formation at a rural/coastal site in Pearl River Delta (PRD) of China, Atmos. Environ., 42, 6275-6283, 10.1016/j.atmosenv.2008.01.063, 2008.

Liu, X. H., Zhu, Y. J., Zheng, M., Gao, H. W., and Yao, X. H.: Production and growth of new particles during two cruise campaigns in the marginal seas of China, Atmos. Chem. Phys., 14, 7941-7951, 10.5194/acp-14-7941-2014, 2014.

Manninen, H. E., Nieminen, T., Asmi, E., Gagné, S., Häkkinen, S., Lehtipalo, K., Aalto, P., Vana, M., Mirme, A., Mirme, S., Hõrrak, U., Plass-Dülmer, C., Stange, G., Kiss, G., Hoffer, A., Törő, N., Moerman, M., Henzing, B., de Leeuw, G., Brinkenberg, M., Kouvarakis, G. N., Bougiatioti, A., Mihalopoulos, N., O'Dowd, C., Ceburnis, D., Arneth, A., Svenningsson, B., Swietlicki, E., Tarozzi, L., Decesari, S., Facchini, M. C., Birmili, W., Sonntag, A., Wiedensohler, A., Boulon, J., Sellegri, K., Laj, P., Gysel, M., Bukowiecki, N., Weingartner, E., Wehrle, G., Laaksonen, A., Hamed, A., Joutsensaari, J., Petäjä, T., Kerminen, V. M., and Kulmala, M.: EUCAARI ion spectrometer measurements at 12 European sites-analysis of new particle formation events, Atmos. Chem. Phys., 10, 7907-7927, 10.5194/acp-10-7907-2010, 2010.

Mikkonen, S., Romakkaniemi, S., Smith, J. N., Korhonen, H., Petäjä, T., Plass-Duelmer, C., Boy, M., McMurry, P. H., Lehtinen, K. E. J., Joutsensaari, J., Hamed, A., Mauldin Iii, R. L., Birmili, W., Spindler, G., Arnold, F., Kulmala, M., and Laaksonen, A.: A statistical proxy for sulphuric acid concentration, Atmos. Chem. Phys., 11, 11319-11334, 10.5194/acp-11-11319-2011, 2011.

Peng, J. F., Hu, M., Wang, Z. B., Huang, X. F., Kumar, P., Wu, Z. J., Guo, S., Yue, D. L., Shang, D. J., Zheng, Z., and He, L.

Y.: Submicron aerosols at thirteen diversified sites in China: size distribution, new particle formation and corresponding contribution to cloud condensation nuclei production, Atmos. Chem. Phys., 14, 10249-10265, 10.5194/acp-14-10249-2014, 2014.

Qi, X. M., Ding, A. J., Nie, W., Petäjä, T., Kerminen, V. M., Herrmann, E., Xie, Y. N., Zheng, L. F., Manninen, H., Aalto, P., Sun, J. N., Xu, Z. N., Chi, X. G., Huang, X., Boy, M., Virkkula, A., Yang, X. Q., Fu, C. B., and Kulmala, M.: Aerosol size distribution and new particle formation in western Yangtze River Delta of China: two-year measurement at the SORPES station, Atmos. Chem. Phys., 15, 12491-12537, 10.5194/acpd-15-12491-2015, 2015.

Rose, C., Sellegri, K., Asmi, E., Hervo, M., Freney, E., Colomb, A., Junninen, H., Duplissy, J., Sipilä, M., Kontkanen, J., Lehtipalo, K., and Kulmala, M.: Major contribution of neutral clusters to new particle formation at the interface between the boundary layer and the free troposphere, Atmos. Chem. Phys., 15, 3413-3428, 10.5194/acp-15-3413-2015, 2015.

Saunders, R. W., Kumar, R., Martin, J. C. G., Mahajan, A. S., Murray, B. J., and Plane, J. M. C.: Studies of the Formation and Growth of Aerosol from Molecular Iodine Precursor, Z. Phys. chem., 224, 1095-1117, 10.1524/zpch.2010.6143, 2010.

Shen, X. J., Sun, J. Y., Zhang, X. Y., Zhang, Y. M., Zhang, L., Fan, R. X., Zhang, Z. X., Zhang, X. L., Zhou, H. G., Zhou, L. Y., Dong, F., and Shi, Q. F.: The influence of emission control on particle number size distribution and new particle formation during China's V-Day parade in 2015, Sci. Total Environ., 573, 409-419, 10.1016/j.scitotenv.2016.08.085, 2016.

Sihto, S.-L., Kulmala, M., Kerminen, V.-M., Dal Maso, M., Petäjä, T., Riipinen, I., Korhonen, H., Arnold, F., Janson, R., Boy, M., Laaksonen, A., and Lehtinen, K. E. J.: Atmospheric sulphuric acid and aerosol formation implications from atmospheric measurements for nucleation and early growth mechanisms, Atmos. Chem. Phys., 6, 4079-4091, 10.5194/acp-6-4079-2006, 2006.

Song, M., Lee, M., Kim, J. H., Yum, S. S., Lee, G., and Kim, K.-R.: New particle formation and growth in relation to vertical mixing and chemical species during ABC-EAREX2005, Atmos. Res., 97, 359-370, 10.1016/j.atmosres.2010.04.013, 2010.

Sorribas, M., Adame, J. A., Olmo, F. J., Vilaplana, J. M., Gil-Ojeda, M., and Alados-Arboledas, L.: A long-term study of new particle formation in a coastal environment: meteorology, gas phase and solar radiation implications, Sci. Total Environ., 511, 723-737, 10.1016/j.scitotenv.2014.12.011, 2015.

Spracklen, D. V., Carslaw, K. S., Kulmala, M., Kerminen, V.-M., Sihto, S.-L., Riipinen, I., Merikanto, J., Mann, G. W., Chipperfield, M. P., Wiedensohler, A., Birmili, W., and Lihavainen, H.: Contribution of particle formation to global cloud condensation nuclei concentrations, Geophys. Res. Lett., 35, 160-162, 10.1029/2007gl033038, 2008.

Sun, L., Xue, L. K., Wang, T., Gao, J., Ding, A. J., Cooper, O. R., Lin, M. Y., Xu, P. J., Wang, Z., Wang, X. F., Wen, L., Zhu, Y. H., Chen, T. S., Yang, L. X., Wang, Y., Chen, J. M., and Wang, W. X.: Significant increase of summertime ozone at Mount Tai in Central Eastern China, Atmos. Chem. Phys., 16, 10637-10650, 10.5194/acp-16-10637-2016, 2016.

Venzac, H., Sellegri, K., Laj, P., Villani, P., Bonasoni, P., Marinoni, A., Cristofanelli, P., Calzolari, F., Fuzzi, S., Decesari, S., Facchini, M. C., Vuillermoz, E., and Verza, G. P.: High frequency new particle formation in the Himalayas, Proc. Natl. Acad.

Sci. USA, 105, 15666-15671, 10.1073/pnas.0801355105, 2008.

Wang, D. W., Guo, H., Cheung, K., and Gan, F. X.: Observation of nucleation mode particle burst and new particle formation events at an urban site in Hong Kong, Atmos. Environ., 99, 196-205, 10.1016/j.atmosenv.2014.09.074, 2014a.

Wang, H., Zhu, B., Shen, L., An, J., Yin, Y., and Kang, H.: Number size distribution of aerosols at Mt. Huang and Nanjing in the Yangtze River Delta, China: Effects of air masses and characteristics of new particle formation, Atmos. Res., 150, 42-56, 10.1016/j.atmosres.2014.07.020, 2014b.

Wang, Z. B., Hu, M., Yue, D. L., Zheng, J., Zhang, R. Y., Wiedensohler, A., Wu, Z. J., Nieminen, T., and Boy, M.: Evaluation on the role of sulfuric acid in the mechanisms of new particle formation for Beijing case, Atmos. Chem. Phys., 11, 12663-12671, 10.5194/acp-11-12663-2011, 2011.

Wang, Z. B., Hu, M., Wu, Z. J., and Yue, D. L.: Reasearch on the Formation Mechanisms of New Particles in the Atmosphere, Acta. Chim. Sinica, 71, 519-527, 10.6023/a12121062, 2013.

Wang, Z. B., Hu, M., Pei, X. Y., Zhang, R. Y., Paasonen, P., Zheng, J., Yue, D. L., Wu, Z. J., Boy, M., and Wiedensohler, A.: Connection of organics to atmospheric new particle formation and growth at an urban site of Beijing, Atmos. Environ., 103, 7-17, 10.1016/j.atmosenv.2014.11.069, 2015.

Wehner, B., Wiedensohler, A., Tuch, T. M., Wu, Z. J., Hu, M., Slanina, J., and Kiang, C. S.: Variability of the aerosol number size distribution in Beijing, China: New particle formation, dust storms, and high continental background, Geophys. Res. Lett., 31, L22108, 10.1029/2004gl021596, 2004.

Weingartner, E., Nyeki, S., and Baltensperger, U.: Seasonal and diurnal variation of aerosol size distributions (10<D<750 nm) at a high-alpine site (Jungfraujoch 3580 m asl), J. Geophys. Res., 104, 26809-26820, 10.1029/1999jd900170, 1999.

Wu, Z., Hu, M., Liu, S., Wehner, B., Bauer, S., Ma ßling, A., Wiedensohler, A., Petäjä, T., Dal Maso, M., and Kulmala, M.: New particle formation in Beijing, China: Statistical analysis of a 1-year data set, J. Geophys. Res., 112, 9209, 10.1029/2006jd007406, 2007.

Xiao, S., Wang, M. Y., Yao, L., Kulmala, M., Zhou, B., Yang, X., Chen, J. M., Wang, D. F., Fu, Q. Y., Worsnop, D. R., and Wang, L.: Strong atmospheric new particle formation in winter in urban Shanghai, China, Atmos. Chem. Phys., 15, 1769-1781, 10.5194/acp-15-1769-2015, 2015.

Yue, D. L., Hu, M., Zhang, R. Y., Wang, Z. B., Zheng, J., Wu, Z. J., Wiedensohler, A., He, L. Y., Huang, X. F., and Zhu, T.: The roles of sulfuric acid in new particle formation and growth in the mega-city of Beijing, Atmos. Chem. Phys., 10, 4953-4960, 10.5194/acp-10-4953-2010, 2010.

Yue, D. L., Hu, M., Wang, Z. B., Wen, M. T., Guo, S., Zhong, L. J., Wiedensohler, A., and Zhang, Y. H.: Comparison of particle number size distributions and new particle formation between the urban and rural sites in the PRD region, China, Atmos. Environ., 76, 181-188, 10.1016/j.atmosenv.2012.11.018, 2013.

Zhang, R., Suh, I., Zhao, J., Zhang, D., Fortner, E. C., Tie, X., Molina, L. T., and Molina, M. J.: Atmospheric new particle

formation enhanced by organic acids, Science, 304, 1487-1490, 10.1126/science.1095139, 2004.

Zhang, R.: Getting to the Critical Nucleus of Aerosol Formation, Science, 328, 1366-1367, 2010.

Zhang, R., Khalizov, A., Wang, L., Hu, M., and Xu, W.: Nucleation and growth of nanoparticles in the atmosphere, Chem. Rev., 112, 1957-2011, 10.1021/cr2001756, 2012.

Zhang, X., Yin, Y., Lin, Z., Han, Y., Hao, J., Yuan, L., Chen, K., Chen, J., Kong, S., Shan, Y., Xiao, H., and Tan, W.: Observation of aerosol number size distribution and new particle formation at a mountainous site in Southeast China, Sci. Total Environ., 575, 309-320, 10.1016/j.scitotenv.2016.09.212, 2016.

Zhang, X. H., Zhang, Y. M., Sun, J. Y., Zheng, X. J., Li, G., and Deng, Z. Q.: Characterization of particle number size distribution and new particle formation in an urban environment in Lanzhou, China, J. Aerosol Sci., 103, 53-66, 10.1016/j.jaerosci.2016.10.010, 2017.

Zhang, Y. M., Zhang, X. Y., Sun, J. Y., Lin, W. L., Gong, S. L., Shen, X. J., and Yang, S.: Characterization of new particle and secondary aerosol formation during summertime in Beijing, China, Tellus B, 63, 382-394, 10.1111/j.1600-0889.2011.00533.x, 2011.

Zhang, Y. M., Zhang, X. Y., Sun, J. Y., Hu, G. Y., Shen, X. J., Wang, Y. Q., Wang, T. T., Wang, D. Z., and Zhao, Y.: Chemical composition and mass size distribution of PM1 at an elevated site in central east China, Atmos. Chem. Phys., 14, 12237-12249, 10.5194/acp-14-12237-2014, 2014.

Zhu, Y., Sabaliauskas, K., Liu, X., Meng, H., Gao, H., Jeong, C.-H., Evans, G. J., and Yao, X.: Comparative analysis of new particle formation events in less and severely polluted urban atmosphere, Atmos. Environ., 98, 655-664, 10.1016/j.atmosenv.2014.09.043, 2014.

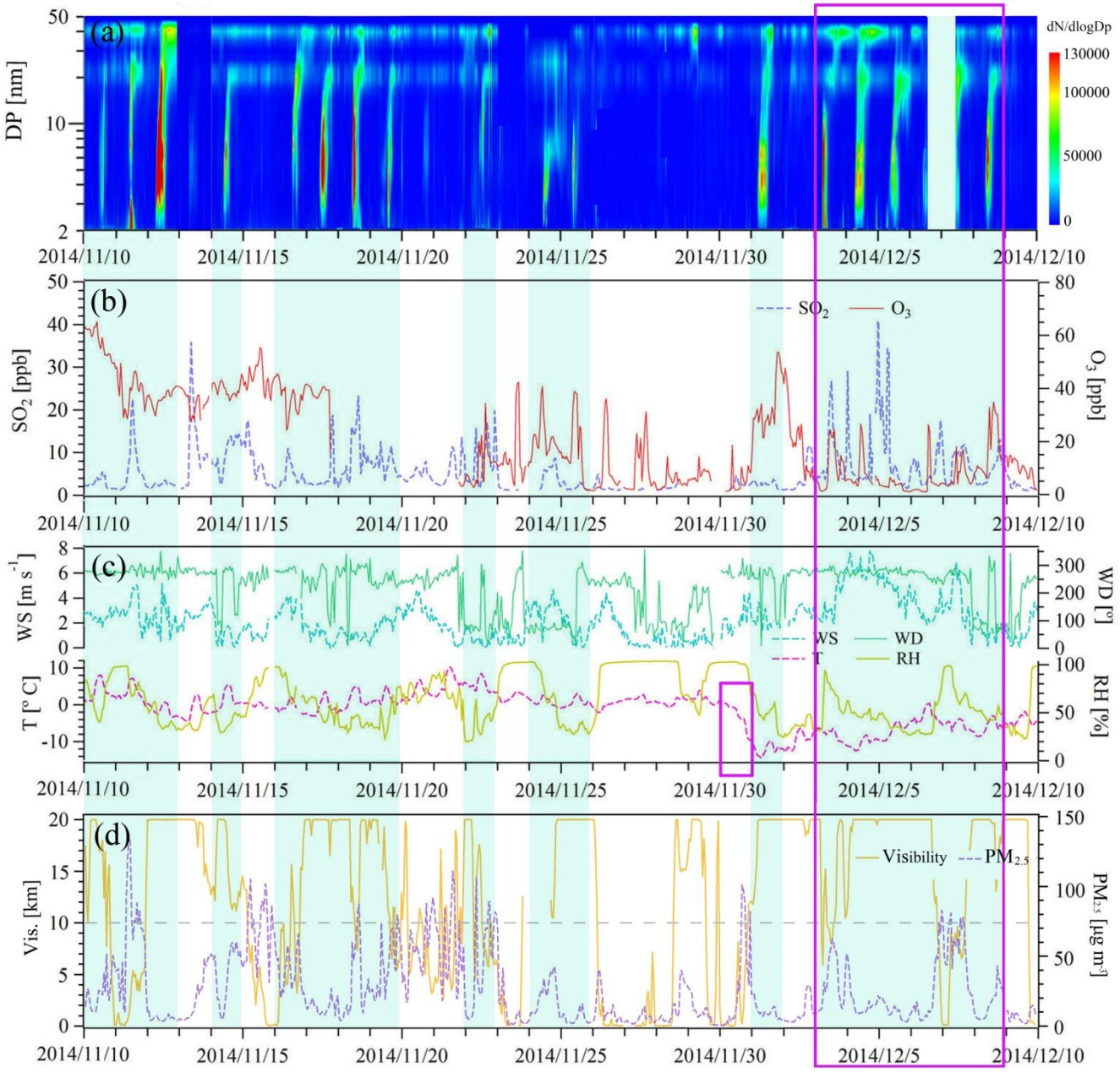

Fig. 1. Time series during 10 November-9 December 2014, and the shaded areas represent the NPF days: (a) contour plot of particle number size distribution using NAIS data; (b) sulfur dioxide (blue) and ozone (red); (c) meteorological parameters, including wind speed (cyan), wind direction (green), temperature (magenta) and relative humidity (earth yellow); (d) visibility (yellow) and $PM_{2.5}$ concentration (purple), and the gray line is the boundary for 10 km and 75 μg m^{-3}.

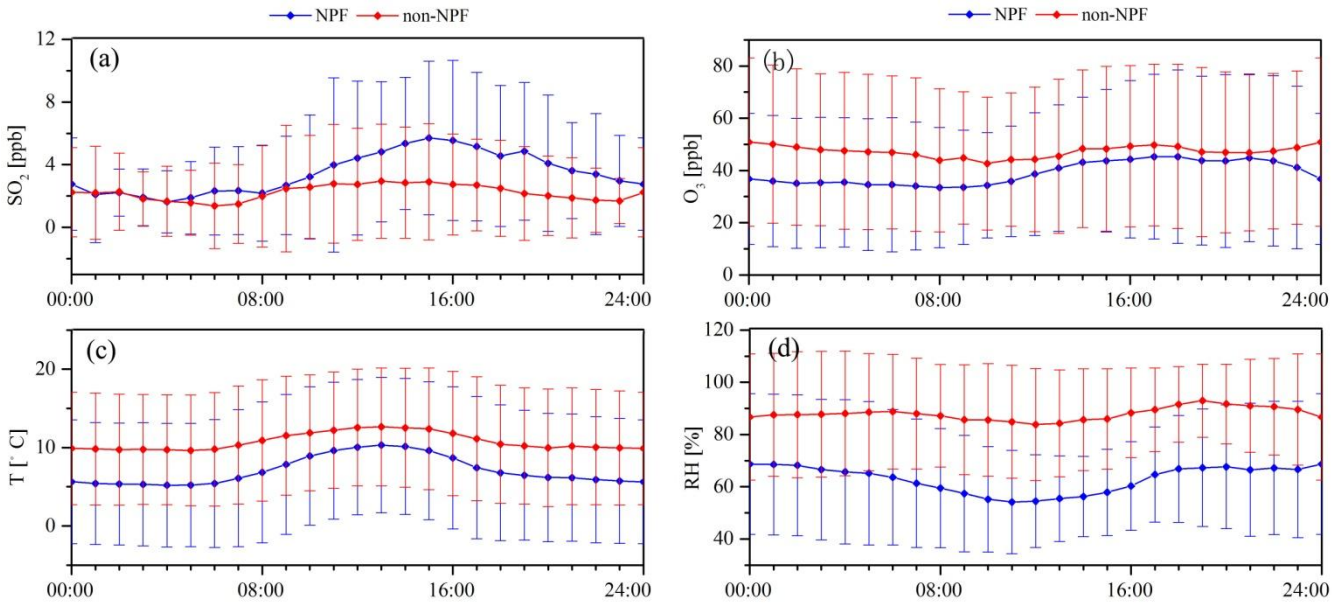

Fig. 2. Average diurnal variations of trace gases (SO_2 and O_3) and meteorological conditions (T and RH) on NPF days and non-NPF days over all the campaigns at the summit of Mt. Tai

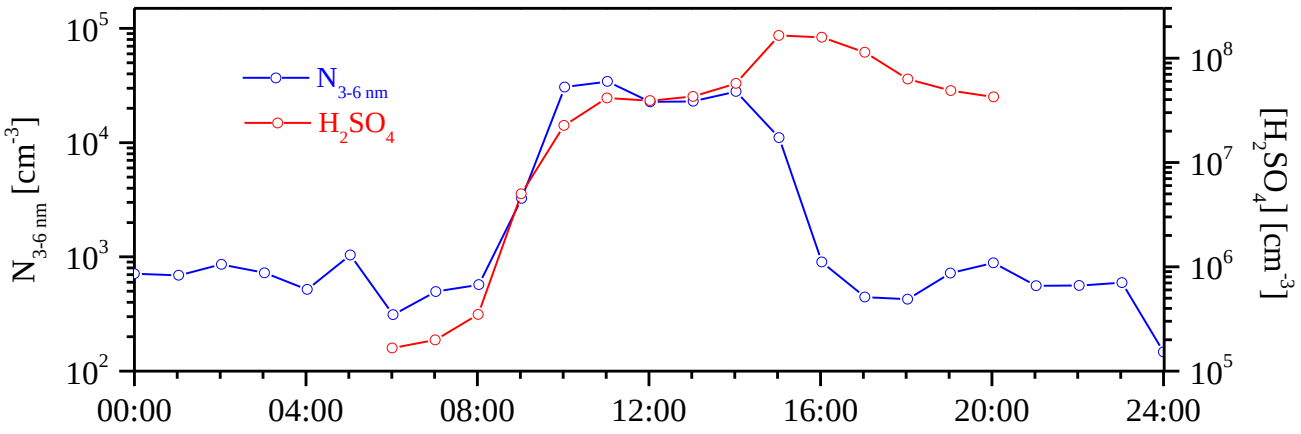

Fig. 3. The particle number concentration of 3-6 nm ($N_{3\text{-}6}$, blue) and sulfuric acid proxy concentration ([H_2SO_4], red) on 14 October 2014, fitting a good relationship (R^2 =0.975) between 6:00-14:00 LT during the NPF event.

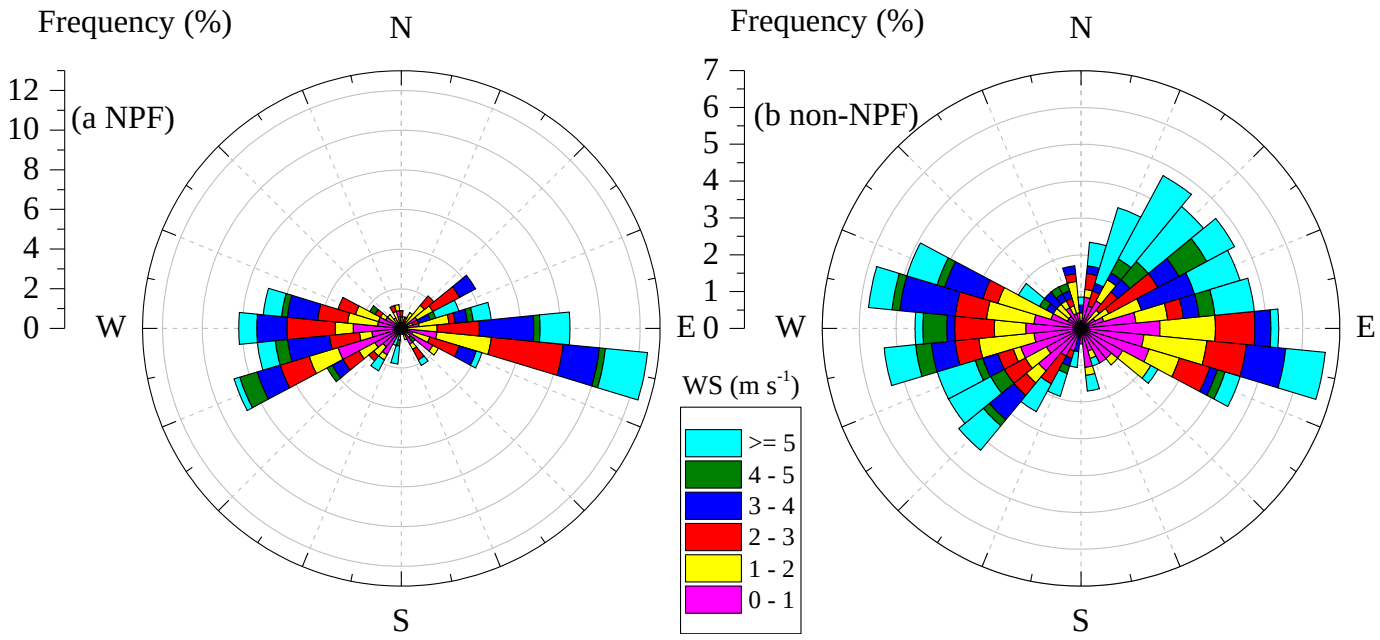

Fig. 4. Wind rose plots of all NPF days (a) and non-NPF days (b), and wind speed and wind direction between 06:00 and 11:00 LT are included. Length of each spoke on the circle represents the probability of wind coming from a particular direction at the certain range of wind speed.

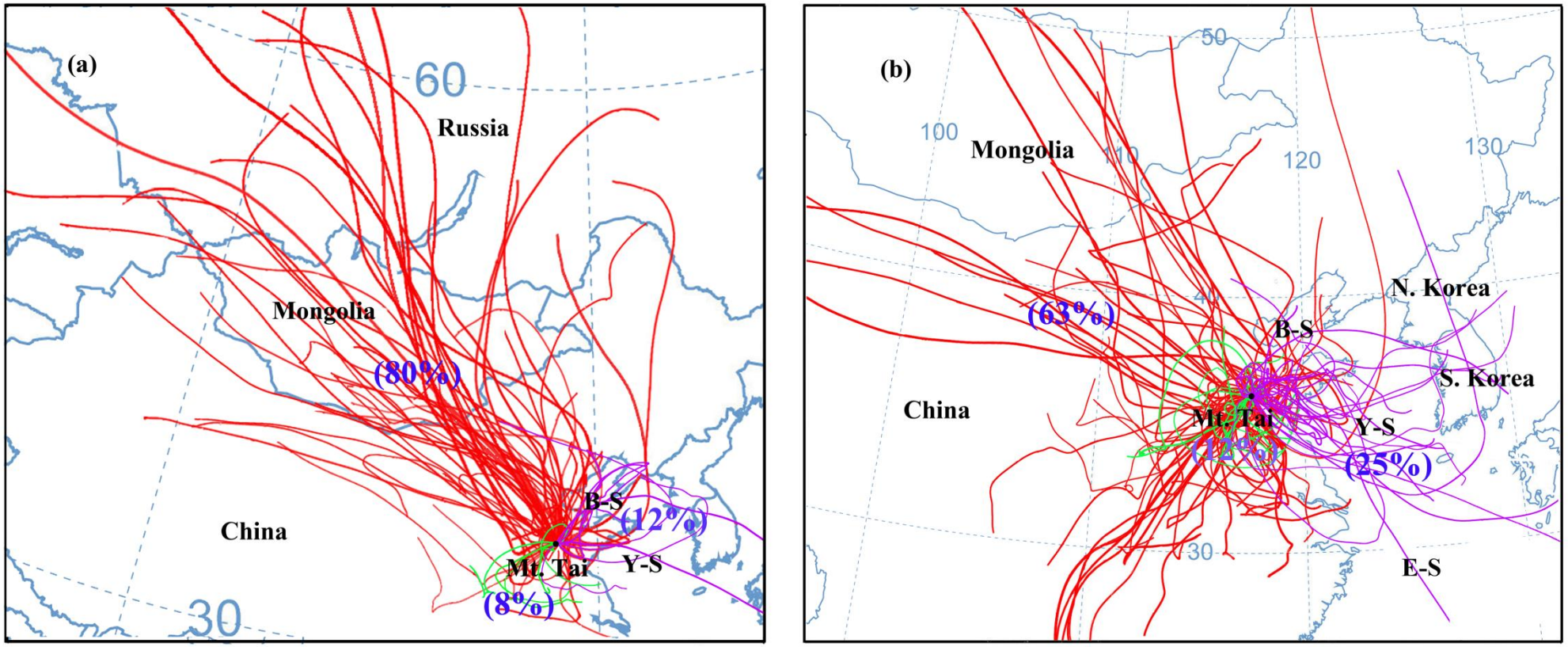

Fig. 5. Air mass back trajectories for 72 h at 6:00 LT at 1535 m ASL on all NPF days (a) and non-NPF days (b), and the continental air mass, local air mass and maritime air mass are represented in red, green and magenta, respectively.

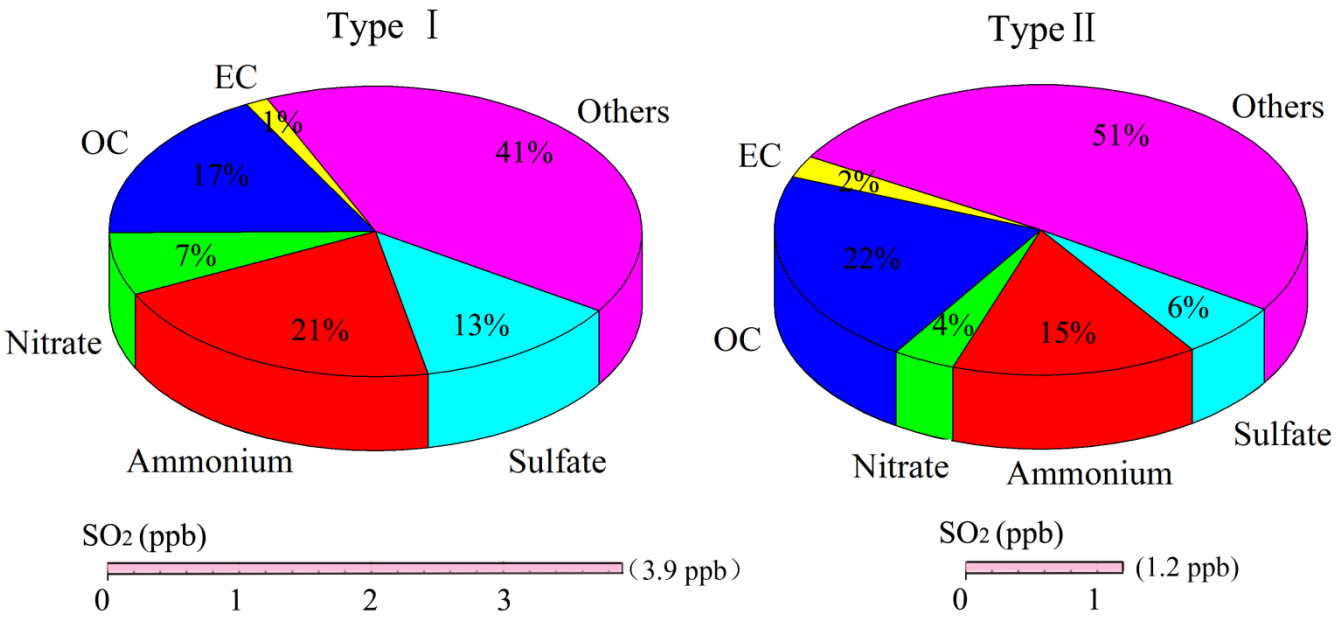

Fig. 6. The average chemical composition of $PM_{2.5}$ and SO_2 concentration in more polluted continental air mass (Type I) and relatively cleaner continental air mass (Type II) on NPF days

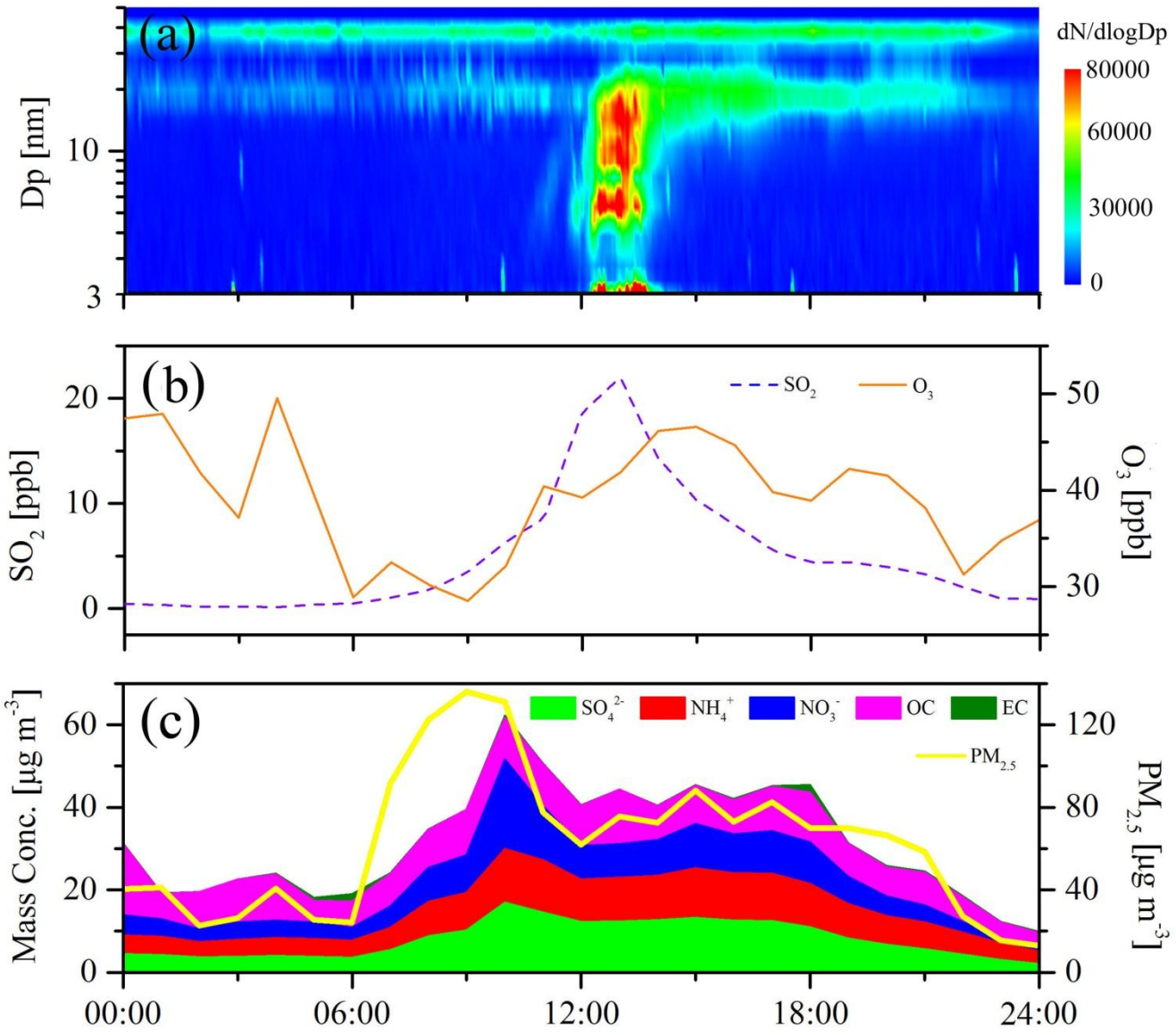

Fig. 7. Time series of particle size distribution, trace gases, chemical composition and mass concentration of $PM_{2.5}$ on 11 November 2014.

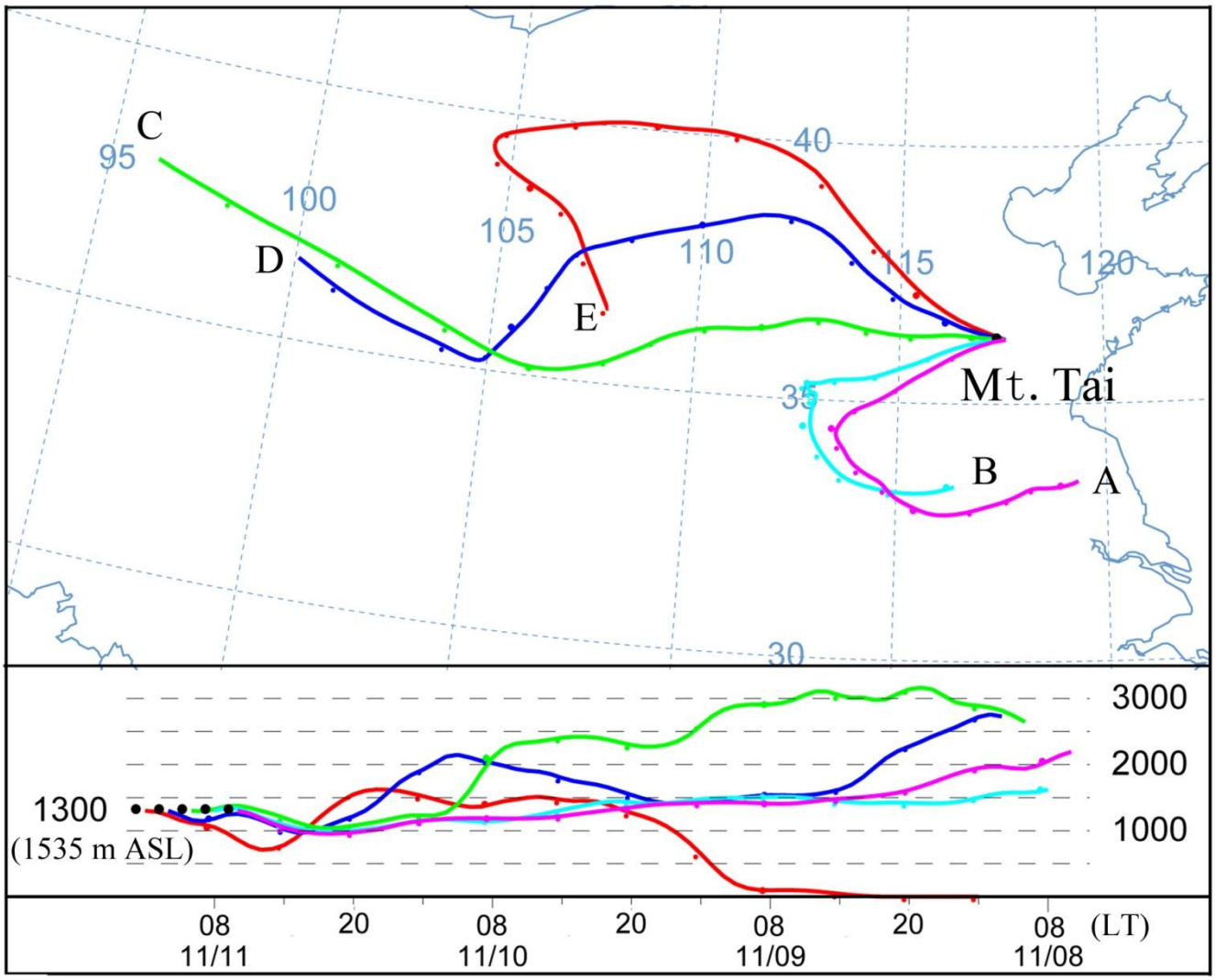

Fig. 8. Air mass backward trajectories for 72 h at 1535 m ASL at 6:00 (A), 8:00 (B), 10:00 (C), 12:00 (D) and 14:00 LT (E) on 11 November 2014.

Table 1. The calculated parameters of all the NPF events during the three campaigns, the minima and maxima are marked in blue and red, respectively

Campaign	Date	J_3 cm^{-3} s^{-1}	$J_{3\text{-}20}$ cm^{-3} s^{-1}	GR $nm\ h^{-1}$	CS 10^{-2} s^{-1}	$[H_2SO_4]$ 10^6 cm^{-3}	SO_2 ppb	O_3 ppb	Date	J_3 cm^{-3} s^{-1}	$J_{3\text{-}20}$ cm^{-3} s^{-1}	GR $nm\ h^{-1}$	CS 10^{-2} s^{-1}	$[H_2SO_4]$ 10^6 cm^{-3}	SO_2 ppb	O_3 ppb
Phase **I**	26-Jul-14	3.34	13.32	1.54	0.5-3.1	N/A	N/A	56±7	8-Aug-14	2.61	16.30	1.15	1.8-15.9	2.87	2.7±2.3	65±10
	27-Jul-14	0.94	6.12	1.55	0.6-2.1	N/A	2.4±2.0	56±9	11-Aug-1	N/A	1.44	1.71	0.2-6.9	3.81	0.6±0.5	56±6
	2-Aug-14	N/A	3.60	3.81	0.1-8.7	N/A	N/A	22±13	12-Aug-1	N/A	40.13	3.69	0.8-7.4	22.1	10.8±7.9	79±16
	3-Aug-14	N/A	1.69	**7.76**	0.1-26.9	N/A	1.5±1.2	35±17	15-Aug-1	2.75	4.52	3.00	N/A	N/A	1.0±1.0	63±12
	6-Aug-14	23.90	52.54	5.78	0.2-1.9	N/A	4.8±2.6	50±5	20-Aug-1	**0.82**	1.33	4.80	0.6-2.7	9.25	5.2±4.3	72±8
	7-Aug-14	N/A	10.90	1.45	0.1-24.8	N/A	1.5±1.7	56±4								
Phase **II**	22-Sep-14	0.99	1.58	1.12	0.7-9.0	7.74	5.7±1.7	76±8	4-Nov-14	7.73	15.06	0.77	0.6-1.5	5.39	6.3±1.2	56±3
	29-Sep-14	16.63	54.97	1.13	0.7-21.1	2.43	1.4±1.1	48±5	6-Nov-14	0.98	**1.10**	1.45	0.1-1.2	2.02	0.6±0.5	13±5
	30-Sep-14	7.94	20.61	1.62	0.5-28.4	1.09	1.9±0.5	2±1	7-Nov-14	1.40	5.59	1.26	0.1-2.0	0.93	0.4±0.3	23±11
	2-Oct-14	5.16	12.02	1.15	0.2-6.6	1.98	1.6±1.7	41±4	8-Nov-14	9.40	13.53	2.95	0.4-2.3	6.71	4.1±2.6	38±3
	3-Oct-14	5.44	14.07	1.50	0.1-4.6	1.34	0.7±0.7	42±3	10-Nov-1	1.02	2.17	3.41	N/A	N/A	2.3±0.7	60±4
	5-Oct-14	8.13	26.41	2.00	0.5-6.9	**0.52**	0.2±0.1	11±5	11-Nov-1	3.29	14.42	2.52	N/A	N/A	7.8±8.3	34±5
	6-Oct-14	2.54	8.94	0.78	0.4-3.4	0.53	0.3±0.4	7±2	12-Nov-1	12.39	26.36	1.09	N/A	N/A	1.6±0.4	35±2
	8-Oct-14	N/A	1.40	0.92	N/A	N/A	5.0±0.6	71±6	14-Nov-1	9.92	13.41	1.55	N/A	N/A	6.1±4.0	40±2
	10-Oct-14	6.54	27.04	1.80	0.2-1.6	4.33	1.8±2.1	54±3	16-Nov-1	5.36	11.06	2.47	0.5-1.2	11.6	5.7±2.9	34±6
	11-Oct-14	9.43	20.37	0.70	0.2-2.2	1.50	3.1±2.5	68±6	17-Nov-1	9.15	16.82	1.10	0.2-0.9	8.38	1.5±0.2	38±2
	13-Oct-14	6.17	26.84	1.64	0.4-2.0	7.43	5.1±1.6	27±8	18-Nov-1	20.45	57.11	0.80	0.1-1.6	4.42	N/A	N/A
	14-Oct-14	10.15	18.11	1.55	0.1-1.4	1.43	0.9±0.8	44±4	19-Nov-1	8.89	15.41	2.51	0.3-2.8	N/A	N/A	N/A
	15-Oct-14	6.76	30.54	2.76	N/A	N/A	10.1±2.9	60±6	22-Nov-1	N/A	11.60	1.23	0.3-5.6	4.18	5.3±4.9	10±8
	16-Oct-14	6.14	36.96	**0.58**	N/A	N/A	1.5±1.9	41±1	24-Nov-1	11.03	24.51	1.50	N/A	N/A	2.9±2.1	26±10
	17-Oct-14	1.55	5.75	2.12	N/A	N/A	N/A	N/A	25-Nov-1	7.11	10.97	2.02	0.1-2.9	N/A	0.5±0.4	25±13
	18-Oct-14	6.16	22.89	2.03	N/A	N/A	N/A	N/A	1-Dec-14	4.96	7.55	1.77	0.1-0.9	1.22	1.4±0.3	27±4
	21-Oct-14	N/A	1.98	2.36	0.4-1.3	N/A	0.3±0.3	13±5	3-Dec-14	**25.04**	**57.43**	1.51	0.4-1.4	1.64	12.9±9.6	13±11
	24-Oct-14	3.64	8.99	1.25	0.5-1.3	1.12	N/A	N/A	4-Dec-14	4.80	10.62	2.69	0.4-1.4	5.48	2.9±0.3	13±9
	25-Oct-14	7.50	14.74	1.60	0.4-1.4	0.89	0.3±0.3	15±11	5-Dec-14	3.34	5.83	1.32	0.2-1.2	0.95	N/A	4±1
	27-Oct-14	7.24	15.49	0.99	N/A	N/A	0.2±0.3	12±4	6-Dec-14	N/A	1.52	1.99	N/A	N/A	2.2±1.2	4±9
	28-Oct-14	2.98	13.17	1.21	N/A	N/A	0.2±0.1	5±2	7-Dec-14	N/A	11.64	1.42	N/A	N/A	7.9±2.5	8±5
	2-Nov-14	11.24	17.78	0.72	0.2-0.9	4.97	0.7±0.1	33±3	8-Dec-14	9.78	16.33	1.24	N/A	N/A	2.4±1.4	16±10
	3-Nov-14	8.77	18.57	1.10	0.3-1.3	6.65	4.6±0.6	37±3								
Phase **III**	16-Jun-15	1.45	9.22	3.98	1.7-4.9	13.6	6.3±0.8	105±7	4-Jul-15	12.55	23.25	0.91	N/A	N/A	5.7±2.9	95±20
	20-Jun-15	6.16	32.50	3.28	0.5-1.8	10.5	2.8±1.6	81±11	8-Jul-15	N/A	8.25	0.93	0.6-2.3	N/A	0.5±0.5	90±16
	21-Jun-15	3.90	6.08	3.44	1.4-3.0	**25.7**	10.0±2.1	105±15	13-Jul-15	N/A	5.64	1.95	1.0-2.4	1.10	0.1±0.1	110±15
	2-Jul-15	9.61	43.41	1.08	0.2-1.9	N/A	2.2±1.3	69±10	15-Jul-15	N/A	19.72	2.86	0.7-1.6	N/A	0.2±0.1	88±12
	3-Jul-15	5.54	10.86	2.65	0.2-2.1	N/A	5.5±2.5	101±13	25-Jul-15	N/A	19.56	1.88	0.4-1.9	2.41	0.3±0.2	99±9

Table 2. Summary of averages, medians, 25th percentiles, 75th percentiles, minima and maxima for the calculated parameters on the basis of Table 1

	Average	Minimum	Maximum	25th percentile	Median	75th percentile
J_3 (cm^{-3} s^{-1})	7.10	0.82	25.04	3.31	6.15	9.41
$J_{3\text{-}20}$ (cm^{-3} s^{-1})	16.61	1.10	57.43	6.12	13.47	20.61
GR ($nm\ h^{-1}$)	1.98	0.58	7.76	1.15	1.55	2.51
CS (10^{-2} s^{-1})	1.4	0.1	28.4	0.5	0.9	1.7
$[H_2SO_4]$ (10^6 cm^{-3})	5.23	0.52	25.7	1.28	3.34	7.07
SO_2 (ppb)	3.2	0.1	12.9	0.7	2.2	2.7
O_3 (ppb)	45	2	110	19	41	66

Table 3. Comparison of NPF characteristics between Mt. Tai and other studies in China

Observation site	FR (cm^{-3} s^{-1})	GR (nm h^{-1})	Freq.	Data	Air mass style	Ref.
Mt. Tai	7.10±5.39 (J_3)	1.98±1.27 (GR_{3-20})	40 %	Jul-Dec 2014 & Jun-Aug 2015	Mountain (1534 m ASL)	This study
Mt. Tai Mo Shan	0.97-10.2 ($J_{5.5}$)	1.5-8.4 ($GR_{5.5-25}$)	33 %	Oct-Nov 2010	Mountain (640 m ASL)	Guo et al. (2012)
Mt. Huang	0.09-0.30 (J_{10})	1.42-4.53 (GR_{10-20})	37 %	Apr-Jul 2008	Mountain (1840 m ASL)	Zhang et al. (2016)
Mt. Huang		2.29-4.27 (GR_{10-15})	18 %	Sep-Oct 2012	Mountain (869 m ASL)	Hao et al. (2015)
Mt. Daban		0.8-3.2	79 %	Sep-Oct 2013	Mountain (3295 m ASL)	Du et al. (2015)
SouthYellow Sea & East China Sea	0.3-15.2 ($J_{5.6-30}$)	2.5-5.0	16 %	Oct-Nov 2011 & Nov 2012	Marine	Liu et al. (2014)
Backgarden	2.4-4.0 (J_{3-25})	4.0-22.7 (GR_{3-25})	25 %	Jul 2006	Rural	Yue et al. (2013)
Nanjing	2.6 (J_6)	10.4 (GR_{6-30})	44 %	Dec 2011-Nov 2013	Suburban	Qi et al. (2015)
Lanzhou		1.2-16.9 (GR_{10-20})	33 %	Jun-Jul 2006	Suburban	Gao et al. (2012)
Xinken	0.5-5.2 (J_{3-20})	2.2-19.8 (GR_{3-20})	26 %	Oct-Nov 2004	Suburban	Liu et al. (2008)
Shanghai	2.3-19.2 (J_3)	1.9-38.3 (GR_{7-20})	21 %	Nov 2013-Jan 2014	Urban	Xiao et al. (2015)
Nanjing	1.6-6.7 (J_{10-25})	5.6-9.6 (GR_{10-25})	40 %	Jul-Aug 2012	Urban	An et al. (2015)
Beijing	5.0-44.9 (J_3)	1.86-6.7 (GR_{7-30})	26 %	Jul-Sep 2008	Urban	Wang et al. (2015)
Lanzhou	0.2-6.2 ($J_{14.6-25}$)	2.6-12.3 ($GR_{14.6-25}$)	34 %	Aug-Nov 2014	Urban	Zhang et al. (2017)
Qingdao	13.3 ($J_{5.6-30}$)	2.0-10.2	41 %	Apr-May 2010	Urban	Zhu et al. (2014)
Hong Kong	1.9 ($J_{5.5}$)	3.7-8.3 ($GR_{5.5-10}$)	23 %	Dec 2010-Jan 2011	Urban	Wang et al. (2014a)